MARTIN MARIETTA ENERGY SYSTEMS LIBRARIES

3 4456 0263676 1

LACE TR-004
ORNL/M-331

ornl

OAK RIDGE
NATIONAL
LABORATORY

MARTIN MARIETTA

Summary of Pretest Aerosol Code Calculations for LWR Aerosol Containment Experiments (LACE) Test LA2

J. H. Wilson
P. C. Arwood

OAK RIDGE NATIONAL LABORATORY
CENTRAL RESEARCH LIBRARY
CIRCULATION SECTION
4500N ROOM
LIBRARY LOAN COPY
DO NOT TRANSFER TO ANOTHER PERSON
If you wish someone else to see this report, send in name with report and the library will arrange a loan.

OPERATED BY
MARTIN MARIETTA ENERGY SYSTEMS, INC.
FOR THE UNITED STATES
DEPARTMENT OF ENERGY

This report was prepared as an account of work sponsored by an agency of the United States Government. Neither the United States Government nor any agency thereof, nor any of their employees, makes any warranty, express or implied, or assumes any legal liability or responsibility for the accuracy, completeness, or usefulness of any information, apparatus, product, or process disclosed, or represents that its use would not infringe privately owned rights. Reference herein to any specific commercial product, process, or service by trade name, trademark, manufacturer, or otherwise, does not necessarily constitute or imply its endorsement, recommendation, or favoring by the United States Government or any agency thereof. The views and opinions of authors expressed herein do not necessarily state or reflect those of the United States Government or any agency thereof.

LACE TR-004
ORNL/M-331

Chemical Technology Division

SUMMARY OF PRETEST AEROSOL CODE CALCULATIONS FOR LWR AEROSOL CONTAINMENT EXPERIMENTS (LACE) TEST LA2

Principal Investigators

J. H. Wilson
P. C. Arwood

Prepared for
ELECTRIC POWER RESEARCH INSTITUTE
3412 Hillview Avenue
Palo Alto, California 94303

EPRI Project No. 2135-18

Date Issued — June 1987

Prepared by the
OAK RIDGE NATIONAL LABORATORY
Oak Ridge, Tennessee 37831
MARTIN MARIETTA ENERGY SYSTEMS, INC.
for the
U.S. DEPARTMENT OF ENERGY
Under Contract DE-AC05-84OR21400

MARTIN MARIETTA ENERGY SYSTEMS LIBRARIES
3 4456 0263676 1

NOTICE

This report was prepared by the organization(s) named below as an account of work sponsored by the Electric Power Research Institute, Inc. (EPRI). Neither EPRI, members of EPRI, the organization(s) named below, nor any person acting on behalf of any of them: (a) makes any warranty, express or implied, with respect to the use of any information, apparatus, method, or process disclosed in this report or that such use may not infringe privately owned rights; or (b) assumes any liabilities with respect to the use of, or for damages resulting from the use of, any information, apparatus, method or process disclosed in this report.

Prepared by

OAK RIDGE NATIONAL LABORATORY
Oak Ridge, Tennessee

[redacted]

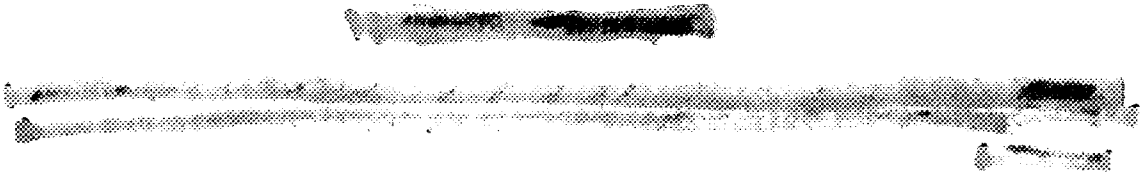

CONTENTS

		Page
ABSTRACT		1
1.	INTRODUCTION	1
2.	SUMMARY OF SPECIFIED INPUTS AND REQUESTED CODE OUTPUTS FOR LA2 PRETEST CALCULATIONS	2
3.	RESULTS OF LA2 PRETEST CALCULATIONS	8
4.	GENERAL COMMENTS ON LA2 PRETEST CALCULATIONS	38
5.	DISCUSSION OF RESULTS OF LA2 PRETEST CALCULATIONS	42
6.	SUMMARY	52
7.	ACKNOWLEDGEMENTS	54
8.	REFERENCES	54
	APPENDIX A	57
	APPENDIX B	58

SUMMARY OF PRETEST AEROSOL CODE CALCULATIONS FOR LWR AEROSOL CONTAINMENT EXPERIMENTS (LACE) TEST LA2

J. H. Wilson
P. C. Arwood

ABSTRACT

This report describes work performed as part of the LWR Aerosol Containment Experiments (LACE) Comparison Coordination Project, which is sponsored by the Electric Power Research Institute (EPRI). The aerosol computer-code pretest calculations performed to model results from the LACE Test LA2 are summarized and compared. The LACE tests are being performed at the Westinghouse Hanford Engineering Development Laboratory (HEDL).

1. INTRODUCTION

The LWR Aerosol Containment Experiments (LACE) are being performed to investigate, on a large scale, aerosol retention behavior in containment under simulated severe reactor accident conditions. An additional objective of these experiments is to provide a data base for validating aerosol containment computer codes and related thermal-hydraulic computer codes. The LACE tests are internationally funded and are being performed at the Hanford Engineering Development Laboratory (HEDL) under the leadership of an overall project board and the Electric Power Research Institute (EPRI).

The LACE project has two components: (1) the experiments being performed at HEDL and (2) aerosol-transport and thermal-hydraulic code-comparison activities. The aerosol-transport code-comparison activities are being coordinated at the Oak Ridge National Laboratory (ORNL), while the thermal-hydraulic code-comparison activities are being coordinated at Intermountain Technologies, Inc. (ITI) in Idaho Falls, Idaho.

For each of the six planned LACE tests, pretest and blind posttest aerosol code calculations will be performed. The activities in the aerosol code-comparison project at ORNL include (1) providing guidance to participating aerosol code analysts to help them in performing pretest and posttest calculations, (2) compiling the results of these calculations, and (3) critically evaluating the results from the aerosol code calculations.

This report summarizes the results from pretest aerosol code calculations performed for test LA2. As defined in the LA2 test plan,[1] this test was designed to simulate a severe accident with a failure to isolate the containment. In the test, aerosol behavior in a large vessel with two pre-existing leak paths was investigated. Aerosol code calculations to model the behavior in the Containment Systems Test Facility (CSTF) vessel were performed. Summaries of the code input conditions specified for the aerosol code calculations and the requested code output results are presented (Sect. 2). In Sects. 3 through 5, the results of the CSTF vessel calculations of various codes are presented and then compared.

2. SUMMARY OF SPECIFIED INPUTS AND REQUESTED OUTPUTS FOR LA2 PRETEST CALCULATIONS

A letter was sent to LACE program participants describing aerosol code inputs and required code outputs for LA2 pretest calculations,[2] and the general contents of this letter are summarized here.

In LACE test LA2, aerosols were generated, transported through a 0.2-m-diam pipe, and injected into the CSTF vessel. Minimal aerosol deposition in the delivery pipe was expected. The behavior of the aerosol in the CSTF vessel, which had two leak paths, was then studied. The expected conditions for test LA2 were defined in the published test plan,[1] which was used to develop the information presented in Table 1. This table summarizes the aerosol-code input parameters required for LA2 pretest calculations. Additional information, as listed below, was supplied to the code users.

1. Predicted temperature, pressure, and leak histories of the CSTF vessel were specified for use in the calculations, as shown in Table 2.
2. To avoid problems such as those experienced in the LA1 pretest calculations (with input of aerosol size parameters to the codes), mass-median diameters were provided for the mixed aerosol and also for MnO and CsOH separately.
3. The collision shape factor and dynamic shape factor were both set equal to 1.

Table 1. Fixed code input parameters for LA2 pretest calculations

CSTF VESSEL PARAMETERS:	
General	
CSTF vessel diameter (ID):	7.62 m
Overall height	20.3 m
Cylinder height	16.5 m
Enclosed volume	852 m^3
Total surface area for aerosol settling	87.8 m^2
Total surface area for wall plateout	741 m^2
Total surface area for heat transfer to environs	520 m^2
(For more detail, see LA2 Test Plan)	
Preexisting Containment Leakpaths	
Upper Leakpath	
Leakpath geometry	Sharp-edged orifice
Orifice diameter	18 mm
Leakpath height above containment bottom	16.5 m
Scrubber flow resistance	8 kPa
Lower Leakpath	
Leakpath geometry	Sharp-edged orifice
Orifice diameter	18 mm
Leakpath height above containment bottom	4.0 m
Scrubber flow resistance	8 kPa
AEROSOL SOURCE CONDITIONS:	
Aerosol injection period to CSTF vessel	0 to 3000 s
CsOH airborne input rate to CSTF vessel	0.6 g/s
MnO airborne input rate to CSTF vessel	1.2 g/s
Aerosol co-agglomeration state at inlet to CSTF vessel	Mixed, aged 13 to 30 s
AMMD of mixed aerosol input to CSTF vessel	2 μm
Geometric standard deviation of mixed aerosol input to CSTF vessel	2
CsOH particle density (1/2 of theoretical)	1.84×10^3 kg/m^3
MnO particle density (1/2 of theoretical)	2.72×10^3 kg/m^3
AEROSOL CARRIER GAS CONDITIONS:	
Steam flow rate	8×10^{-2} kg/s
Nitrogen flow rate	1.25×10^{-1} kg/s
Argon flow rate	1×10^{-2} kg/s
Hydrogen rate	5×10^{-5} kg/s
Carrier gas temperature at containment boundary	553 K
Time for start of carrier gas flow to CSTF vessel	0 s
Time for end of carrier gas flow to CSTF vessel	3000 s

Table 1 (continued)

CSTF VESSEL ATMOSPHERE CONDITIONS:	
Initial	
Gas composition	Normal air
Gas temperature	297 K
Steel temperature	297 K
Pressure, absolute	98.6 kPa
Relative humidity	50 %
Ambient outside temperature	297 K
Sump water mass	1,000 kg
Sump water temperature	297 K
Period 1 (Heatup)	
Start time	-1,800 s
End time	0 s
Steam rate	0.7 kg/s
Steam temperature	423 K
Noncondensible gas rate	0 kg/s
Supplemental containment heat	0 kW
Period 2 (Aerosol Injection)	
Start time	0 s
End time	3,000 s
Steam rate (in addition to aerosol carrier gas)	0.12 kg/s
Steam temperature	423 K
Noncondensible gas rate	0 kg/s
Supplemental containment heat	0 kW
Period 3 (Slow Cooldown)	
Start time	3,000 s
End time	60,000 s
Steam rate	0.02 kg/s
Steam temperature	423 K
Noncondensible gas rate	0 kg/s
Supplemental containment heat	0 kW
Period 4 (Cooldown)	
Start time	60,000 s
End time	170,000 s
Steam rate	0 kg/s
Noncondensible gas rate	0 kg/s

Table 2. Containment conditions and leak rates for use in pretest calculations

Time (s)	Temperature (K)	Pressure (kPa)	Total leak rate[a] m^3/s[b] (at T&P)	Total leak rate[a] Fractional[c] (s^{-1})
-1800	297	98.6		
-1200	316	118	0.0323	3.79E-5
- 600	335	139	0.0554	6.51E-5
0	353	160	0.0581	6.82E-5
600	358	172	0.0626	7.34E-5
1200	363	184	0.0659	7.73E-5
1800	368	196	0.0697	8.18E-5
2400	373	208	0.0725	8.51E-5
3000	378	220	0.0752	8.83E-5
6000	377	214	0.0745	8.75E-5
12000	374	202	0.0714	8.39E-5
18000	371	190	0.0688	8.08E-5
24000	369	178	0.0662	7.76E-5
30000	366	166	0.0622	7.30E-5
36000	364	154	0.0579	6.79E-5
42000	361	142	0.0528	6.20E-5
48000	358	130	0.0470	5.52E-5
54000	356	117	0.0361	4.24E-5
60000	353	105	0.0212	2.49E-5
66000	350	98.6	0	0
120000	330	98.6	0	0
170000	320	98.6	0	0

[a]Leak rate through each orifice = 1/2 of total leak rate.
[b]Volumetric leak rate at temperature and pressure of containment.
[c]Fractional leak rate = (total leak rate at temperature and pressure of containment)/(volume of containment). Volume of containment = 852 m^3.

4. For calculating the effect of thermophoresis on aerosol plateout, the temperature difference between the containment atmosphere and the wall of the CSTF vessel was set equal to 4 K.
5. For determining the effect of diffusiophoresis on aerosol plateout, the steam condensation rate as a function of time was specified.
6. Conditions in the CSTF vessel during the test were assumed to be saturated.

The purpose of providing thermal-hydraulic information and specifying certain parameter values for the pretest calculations was to minimize variances in input data, thereby ensuring a meaningful code-comparison effort.

Table 3 presents a summary of the requested code output parameters for LA2 pretest calculations. Some comments on these parameters are included here.

1. For various parameters (such as suspended aerosol concentration and mass of settled aerosol), the code analysts were requested to provide output data for each species (MnO and CsOH). Various plots involving the MnO/CsOH mass ratio are presented in this report for the "multi-component" codes. The data for the "single-component" codes are not included since the calculated ratio was 2:1 (equal to the MnO/CsOH mass ratio in the source) in all cases.

2. If the code calculations indicated water condensation on the airborne aerosols, data concerning the amount of water associated with the aerosols were requested at the specified output times.

3. Included with the aerodynamic mass-median diameter (AMMD), one of the aerosol size parameters requested was the "aerodynamic mean settling diameter." This is defined as

$$d_{as} = \left[\frac{18\mu_f U_s}{g\rho_{pl}}\right]^{0.5} \times 10^4 ,$$

Table 3. Summary of required output parameters for LA2 pretest calculations

CSTF VESSEL CALCULATIONS

Output times, s: 300; 1,200; 2,100; 3,000; 3,300; 3,600; 3,900; 4,200; 4,800; 5,400; 6,000; 6,600; 8,100; 20,000; 60,000; 170,000

Output parameters and units:

1. Suspended CsOH and MnO aerosol mass concentration: provide this for the MIXED aerosol, and for EACH aerosol species, if possible, g/m^3

2. Mass of water condensed onto airborne CsOH and MnO aerosols, g

3. Cumulative CsOH and MnO aerosol mass leaked from vessel through EACH leak path: provide this for the MIXED aerosol and for EACH aerosol species, if possible, g

4. Cumulative CsOH and MnO aerosol mass settled in vessel: provide this for the MIXED aerosol and for EACH aerosol species, if possible, g

5. Cumulative CsOH and MnO aerosol mass plated on vessel walls and ceilings: provide this for the MIXED aerosol and for EACH aerosol species, is possible, g

6. Airborne CsOH and MnO aerosol size parameters: provide the following for the MIXED aerosol and for EACH aerosol species, if possible:

   a. The AERODYNAMIC MASS-MEDIAN DIAMETER — in μm — and the GEOMETRIC STANDARD DEVIATION — dimensionless

   b. The AERODYNAMIC MEAN SETTLING DIAMETER — in μm

   c. "DISCRETE" code users should provide tables of aerosol mass — in g — in each size group for the times 1,000; 3,000; 4,200; 10,000; and 60,000 s.

where

d_{as} = aerodynamic mean settling diameter (μm),

μ_f = fluid viscosity (g/cm·s),

g = gravitational acceleration (cm/s^2),

ρ_1 = 1 g/cm^3 particle density,

U_s = gravity settling velocity (cm/s), defined as

$$U_s = \frac{\text{Aerosol settling deposition flux}}{\text{Aerosol suspended mess concentration}} .$$

4. The users of "discrete" codes were requested to provide us with data on the aerosol mass in the various size groups used in their codes. The information was needed for detailed comparisons of the size distributions calculated by the various discrete codes.

The LA2 participants were also requested to submit a summary of any major input parameter assumptions (other than those specified in the instruction letter) used in their code calculations. This would include parameters such as the assumed value for thermal boundary-layer thickness. In later correspondence,[3] the need for such information was reemphasized. The code users were also requested to provide copies of the actual computer input and output for their codes. Finally, it was requested that the plated aerosol mass be tabulated according to the deposition mechanism.

3. RESULTS OF PRETEST LA2 CALCULATIONS

Pretest calculations for LA2 were performed by nine investigators. Table 4 lists the codes used and the names of the code analysts. The HAA-4 code assumes the aerosol size distribution to be lognormal at all times. The MAAP-2.9 code assumes that the aerosol approaches an asymptotic size distribution. All other codes listed in Table 4 utilize a discrete particle size distribution model. The "multicomponent" CONTAIN and AEROSIM-M codes calculate particle compositions that vary with particle size, whereas for the "single component" codes, the MnO/CsOH ratio is independent of particle size. Also, the two CONTAIN codes predicted condensation of steam onto the aerosol. The MCT-2 code calculations were

Table 4. Summary of codes used for LA2 pretest vessel calculations

Code[1]	Code analyst	Affiliation
AEROSIM-M(UK)	S. A. Ramsdale	United Kingdom, Satety and Reliability Directorate
CONTAIN(ORNL)	M. L. Tobias	United States, Oak Ridge National Laboratory
CONTAIN(UK)	P. N. Smith	United Kingdom, Atomic Energy Authority
HAA-4(US)	E. U. Vaughan	United States, Rockwell International Corporation
MAAP-2.9(SW)	H. Häggblom	Sweden, Studsvik Energiteknik AB
MCT-2(US)	P. Bieniarz	United States, Risk Management Associates
NAUA-5(FN)	J. Makynen	Finland, Technical Research Centre
NAUA-4(US)	R. Sher	United States, Electric Power Research Institute
REMOVAL(JN)	N. Yamano	Japan, Atomic Energy Research Institute

[1]Initials in parenthesis included to indicate country or organization.

for both a "wet" and "dry" case, i.e., steam condensation and no steam condensation, respectively, on the aerosol. All other codes assumed no steam condensation on the aerosol.

Table 5 lists the plating mechanisms invoked by the codes and data concerning values used for boundary-layer thicknesses. Other information is included for better understanding of the characteristics of each code and for use in interpreting the results that follow. The values for the diffusion boundary-layer thickness and the turbulent energy dissipation factor in Table 5 are seen to differ for some of the codes. However, as discussed in Sect. 5, the amounts of aerosol plating by the mechansisms which utilize these parameters were negligible.

The particle-size distribution data were not reported at the requested output times in all cases (see Table 6). Nevertheless, all data are included in the figures that are presented here. (The data are plotted on the figure that corresponds to the nearest requested output time.)

The calculated aerosol concentration in the CSTF vessel is plotted as a function of time in Figs. 1 through 3. The concentration is that of the dry (MnO and CsOH) aerosol in all cases. The vertical line at 3,000 s indicates the end of the aerosol source. In Figs. 2 and 3, the codes are divided into two groups for the purpose of clarity. Figure 4 shows water concentration vs time for the two CONTAIN codes. This is assumed to be water associated with the aerosol. In the actual LA2 test, the amount of water associated with the aerosol will not be measured. Thus, our comparison of the posttest calculations with the experimental results will involve dry aerosol concentrations.

Figure 5 shows the cumulative aerosol mass retained in the CSTF vessel as a function of time. This is equal to the sum of the cumulative settled and plated masses. The cumulative aerosol mass leaked from the CSTF vessel is presented in Fig. 6. The final sum of retained and leaked masses for each code should equal 5,400 g. In Figs. 7 and 8, the cumulative mass of aerosol removed from the CSTF vessel atmosphere by settling and by plating, respectively, is shown for each code as a function of time. The MCT-2 and the MAAP-2.9 codes did not report separate values for plating and settling. The NAUA-5 code reported plating by the

Table 5. Features of computer codes used for LA2 pretest calculations

Feature of Code	CODE								
	AEROSIM-M	CONTAIN(ORNL)	CONTAIN(UK)	HAA-4	MAAP-2.9	MCT-2	NAUA-5	NAUA-4	REMOVAL
Diffusiophoresis[a]	Yes	Yes	Yes	Yes	No	Yes	No	Yes	Yes
Thermophoresis[a]	Yes	Yes	Yes	Yes	Correlation	Yes	No	No	Yes
Diffusion[a,b]	Yes	Yes	Yes	Yes	Correlation	Yes	Yes	Yes	Yes
T.B.L.[c], mm	10			3					2
D.B.L.[d], mm	1	0.01		0.15			0.1	0.1	0.1
Comments[e]	Multicomponent ϵ = 0.39 m2/s3 during aerosol injection Thermophoresis plating area = 520 m2	Multicomponent Calculated thermal-hydraulics Steam condensation on aerosol ϵ = 0.001 m2/s3	Multicomponent Calculated thermal-hydraulics Steam condensation on aerosol	Gravitional collision efficiency = 0.1 Thermophoresis plating area = 653 m2	Settled and plated aerosol masses not reported separately Collision shape factor = 2.5	Settled and plated aerosol masses not reported separately	Leak rate too high from 0 to 3,0000s to		ϵ = 0.1 m2/s3 Thermophoresis plating area = 741 m2

[a]Plating mechanism

[b]Brownian diffusion.

[c]Thermal boundary layer thickness.

[d]Diffusion boundary layer thickness

[e]ϵ = turbulent energy dissipation factor

Table 6. Summary of times reported for particle size distributions

Code	Code output time, s					
Requested time	—	1,000	3,000	4,200	10,000	60,000
AEROSIM-M	—	1,000	3,000	4,200	10,000	60,000
CONTAIN(ORNL)	—	1,000	3,000	4,200	10,000	60,000
CONTAIN(UK)	—	1,000	3,000	4,200	10,000	60,000
HAA-4	—	—	—	—	—	—
MAAP-2.9	—	—	—	—	—	—
MCT-2	—	900	3,000	4,200	9,900	60,000
NAUA-5	304		3,072	—	8,637	69,513
NAUA-4	—	1,000	3,000	4,200	10,000	60,000
REMOVAL	—	1.000	3.000	4.200	10,000	60,000

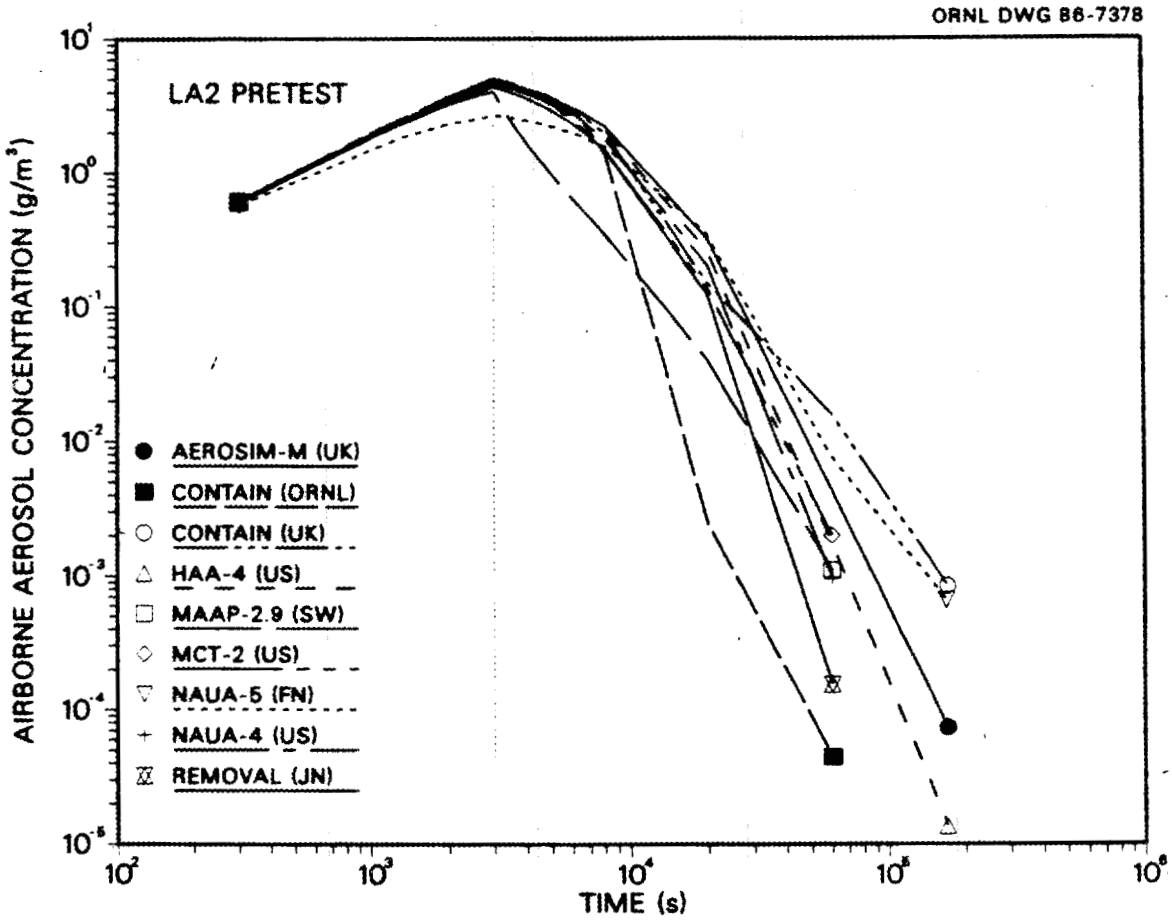

Fig. 1. LA2 pretest calculations — airborne aerosol concentration vs time — for all codes.

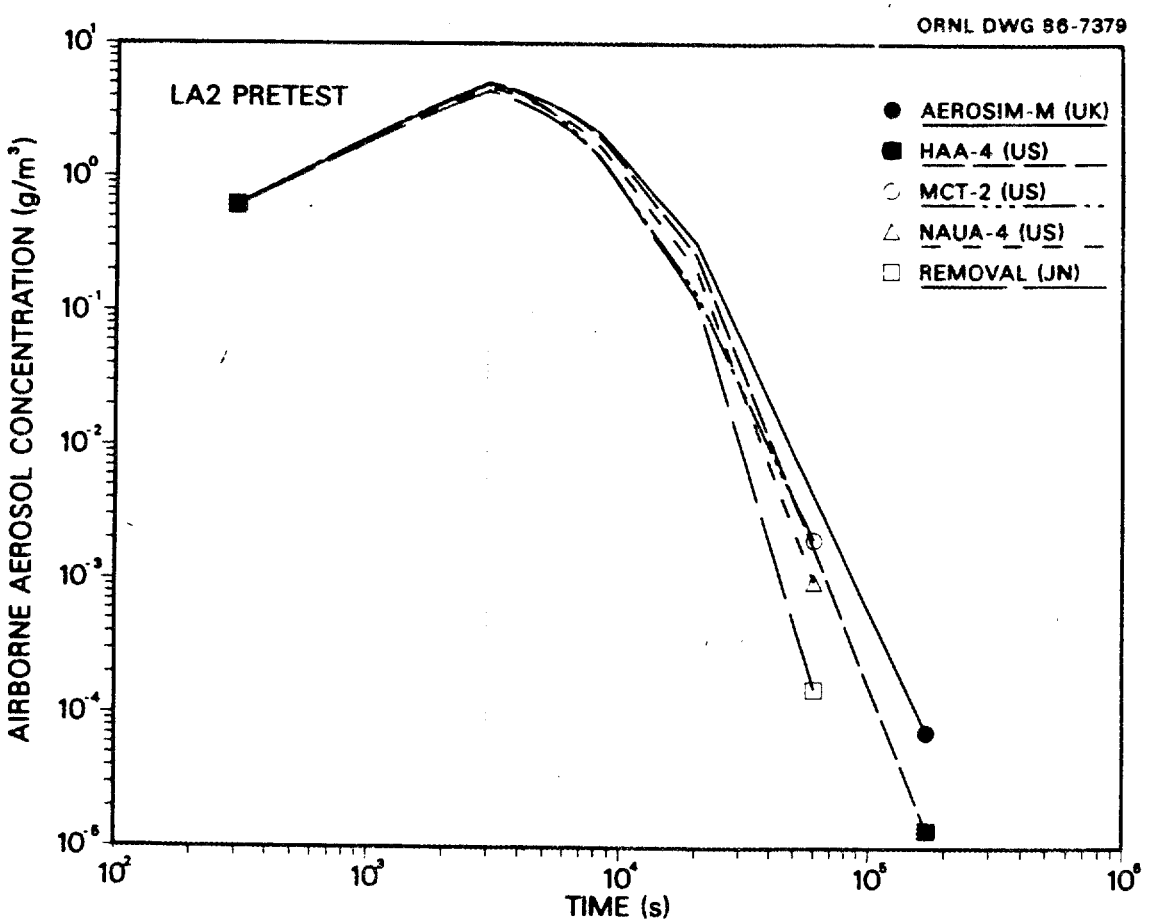

Fig. 2. LA2 pretest calculations — airborne aerosol concentration vs time — for group 1 codes.

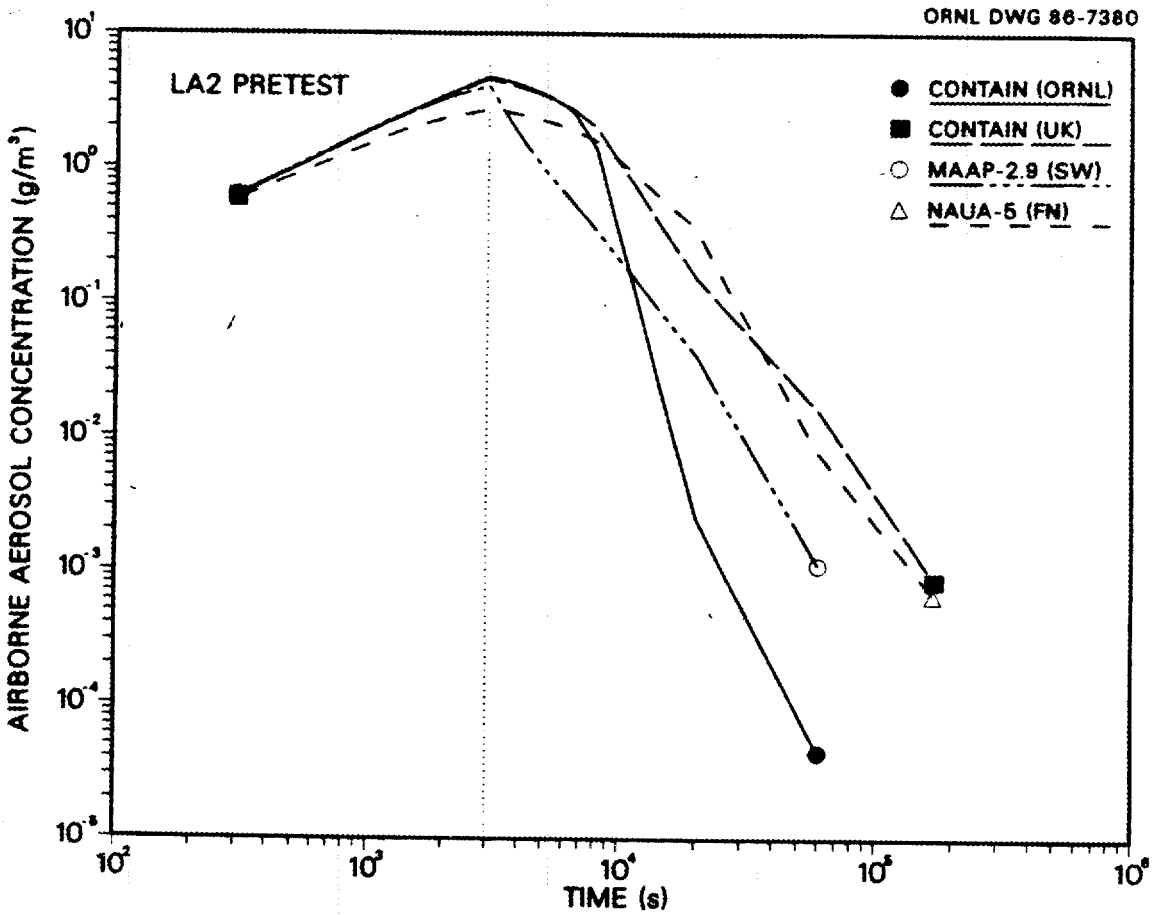

Fig. 3. LA2 pretest calculations — airborne aerosol concentration vs time — for group 2 codes

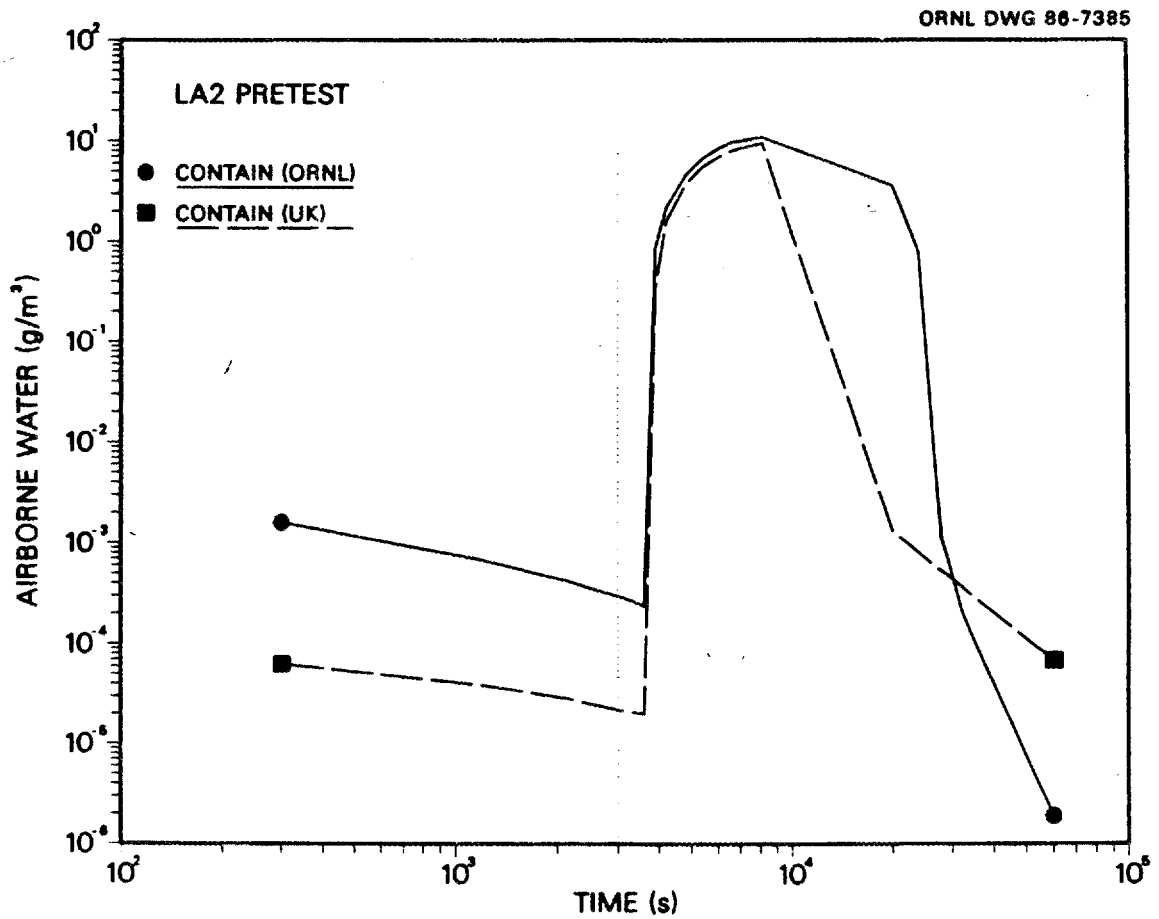

Fig. 4. LA2 pretest calculations — concentration of water condensed on aerosol vs time.

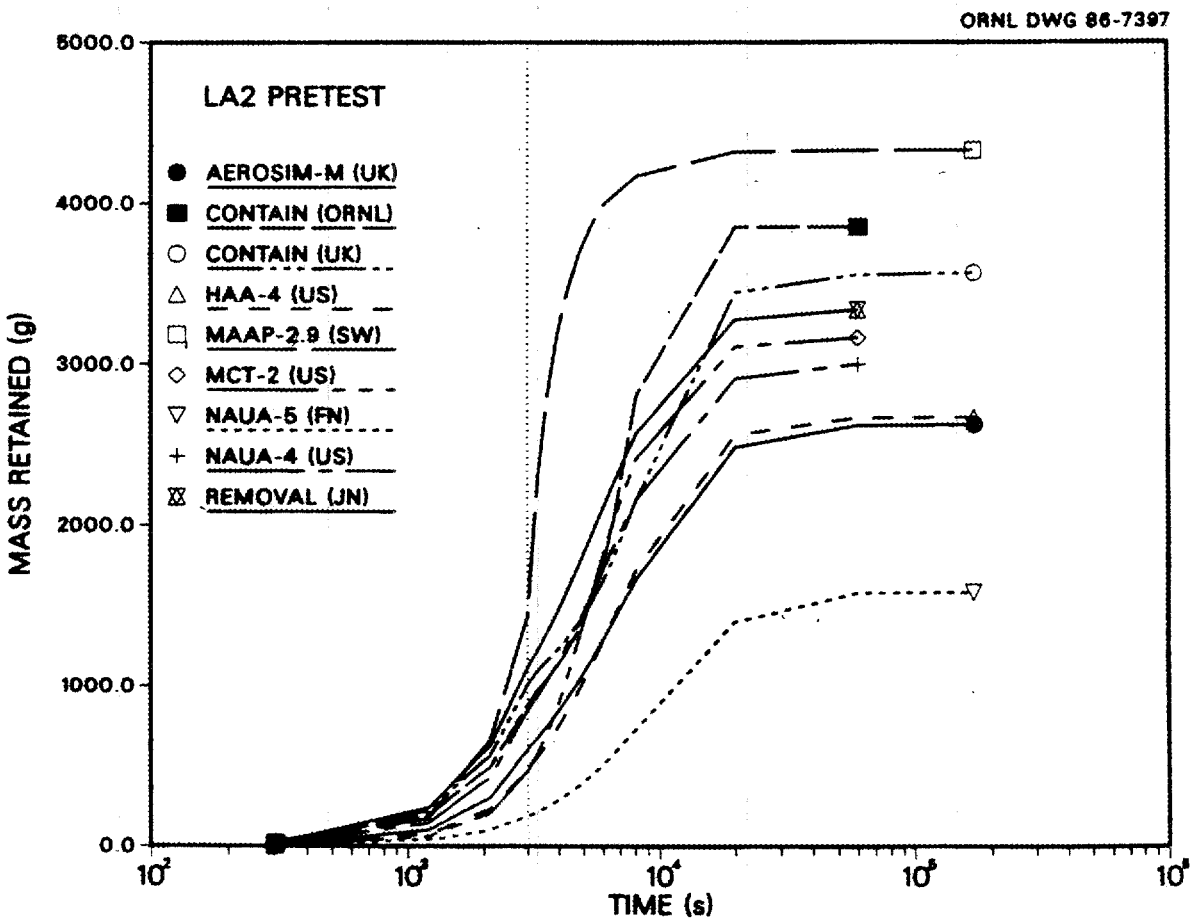

Fig. 5. LA2 pretest calculations — cumulative mass of aerosol retained in CSTF vessel vs time.

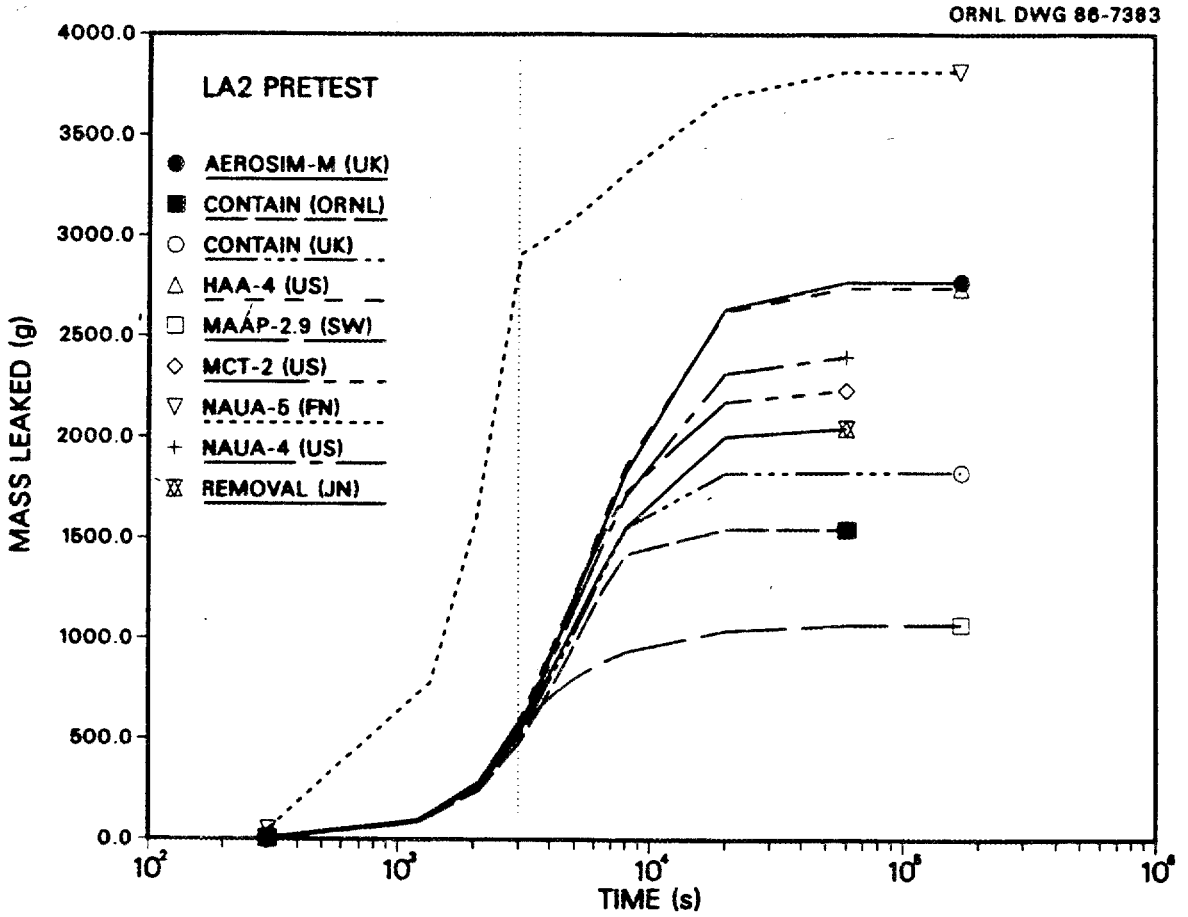

Fig. 6. LA2 pretest calculations — cumulative mass of aerosol leaked from CSTF vessel vs time.

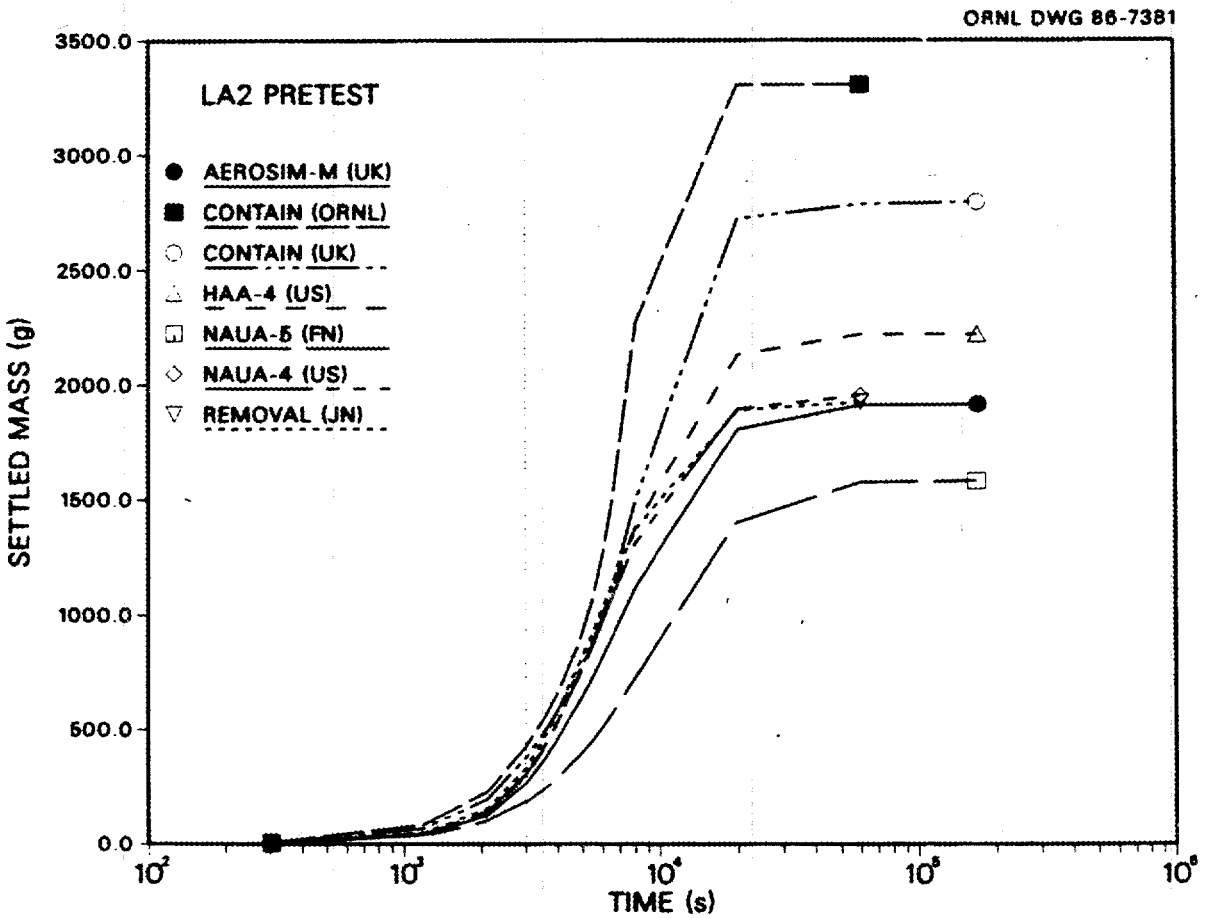

Fig. 7. LA2 pretest calculations — cumulative mass of aerosol settled in CSTF vessel vs time.

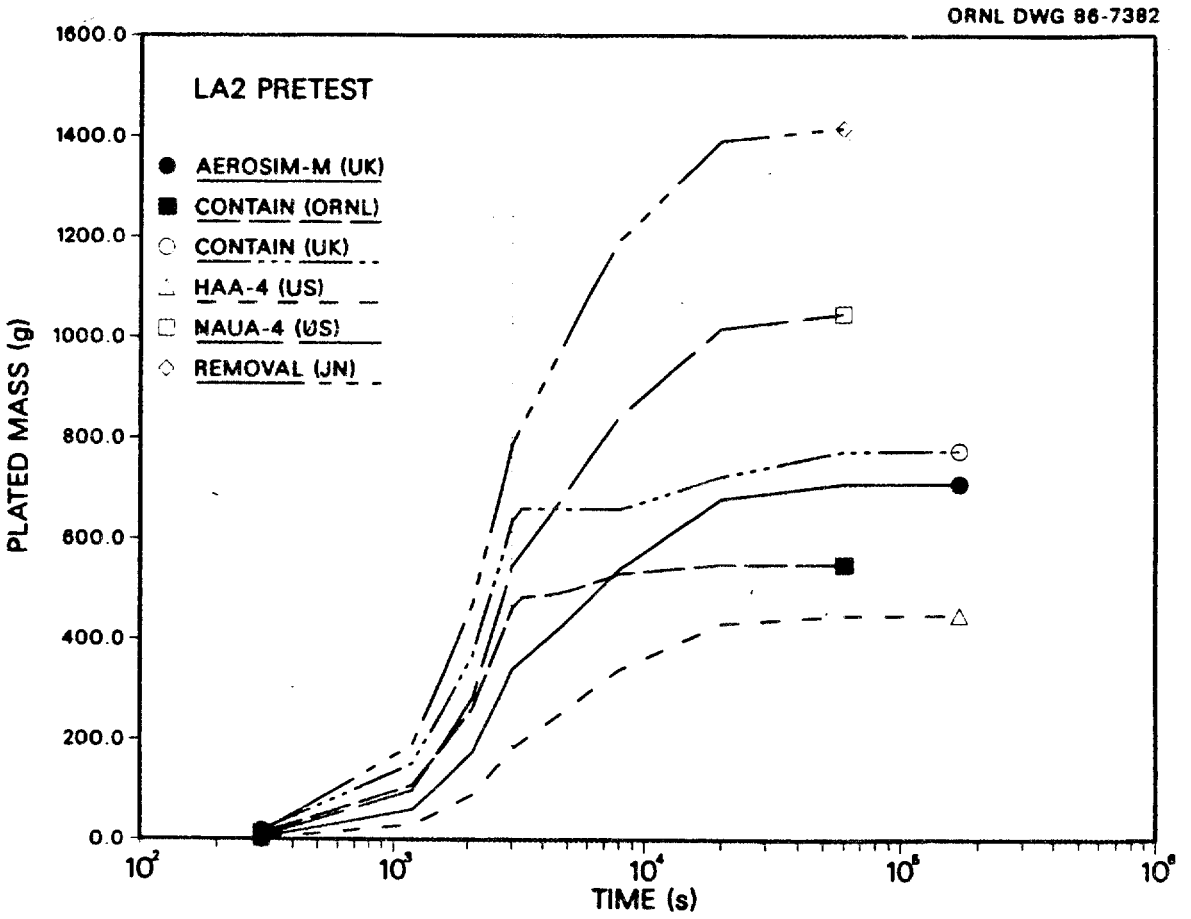

Fig. 8. LA2 pretest calculations — cumulative mass of aerosol plated in CSTF vessel vs time.

Brownian diffusion mechanism only, and only negligible plating was reported. In Figs. 9 and 10, plots are shown for plating by diffusiophoresis and by thermophoresis plus Brownian diffusion, respectively. Four codes provided this type of information (the NAUA-4 code does not include a thermophoresis mechanism).

The AMMD, the geometric standard deviation (GSD), and the aerodynamic mean settling diameter are plotted vs time in Figs. 11 through 13, respectively. The AMMD is expressed as

$$\mathrm{AMMD} = d_{50}\ (\rho/\chi)^{0.5}\ ,$$

where d_{50} is mass-median diameter of the particle size distribution, ρ is the particle density, and χ is the dynamic shape factor. For the CONTAIN codes, the values for AMMD and GSD are for the wet rather than the dry aerosol particles.

Particle size distribution curves are presented in Figs. 14 through 18 for the codes having a discrete distribution model. Each figure shows the distribution for a particular time; in each case the normalized mass fraction of the aerosol in a size interval, or size "bin," is plotted vs the average diameter of particles in that size bin. The dotted vertical line in each drawing represents the d_{50} of the source aerosol. The normalized mass fraction plotted in these figures was determined by dividing the actual mass fraction in each bin (as calculated from the particle size distribution data provided by the codes) by a factor equal to the summation (over all the bins) of the actual mass fraction in each bin times $\Delta\ln(d)$, the latter being the difference between the logarithms of the upper and lower particle diameter limits of the bin. Thus, a particle size distribution curve (which is similar to a probability density function) is generated, making it more meaningful for comparison purposes. The normalized mass fractions in Figs. 14 through 18 correspond to the wet aerosol for the CONTAIN (ORNL) code and to the dry aerosol for the CONTAIN(UK) code [the amount of water associated with each size bin was not provided for the CONTAIN(UK) code]. The distribution curves for both CONTAIN codes in Figs. 14 through 18 are plotted vs the actual diameter of the wet aerosol.

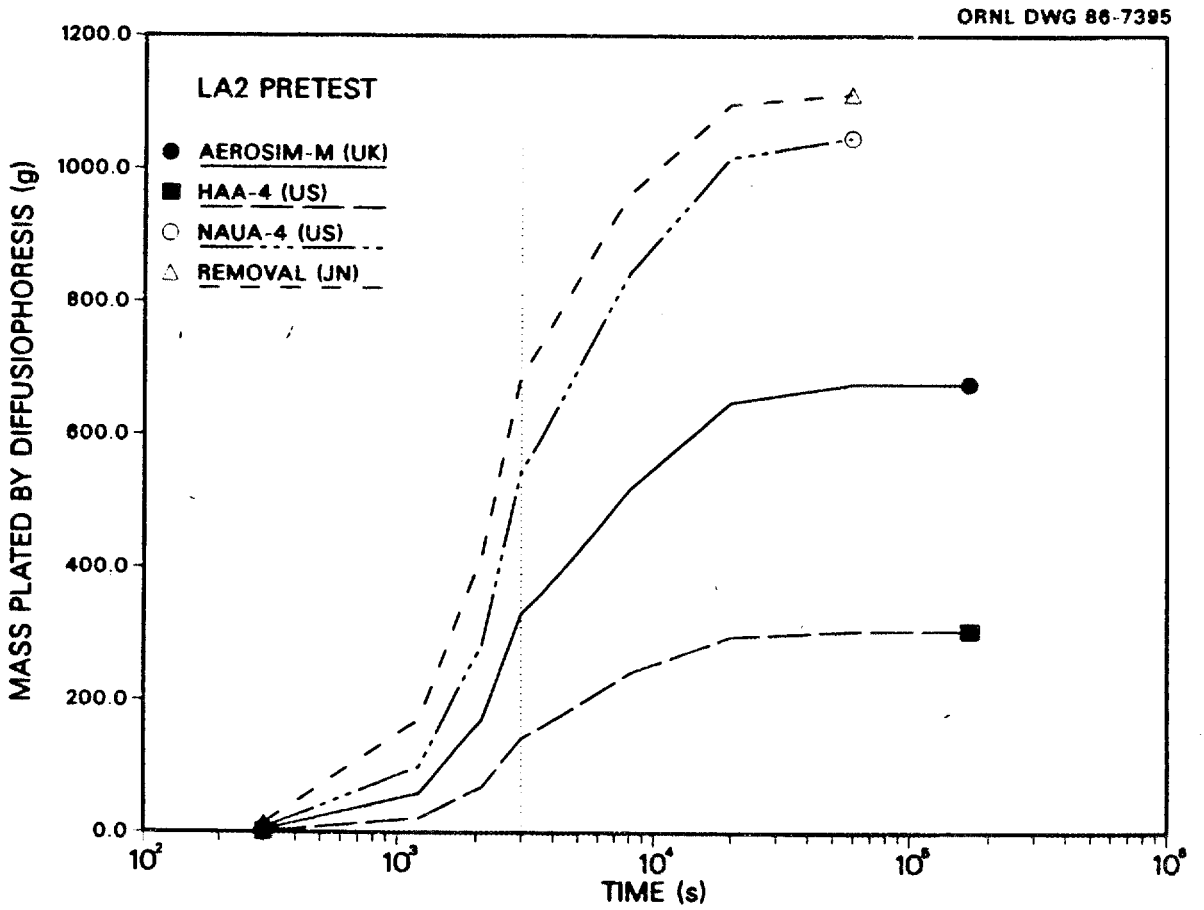

Fig. 9. LA2 pretest calculations — cumulative mass of aerosol plated in CSTF vessel by diffusiophoresis vs time.

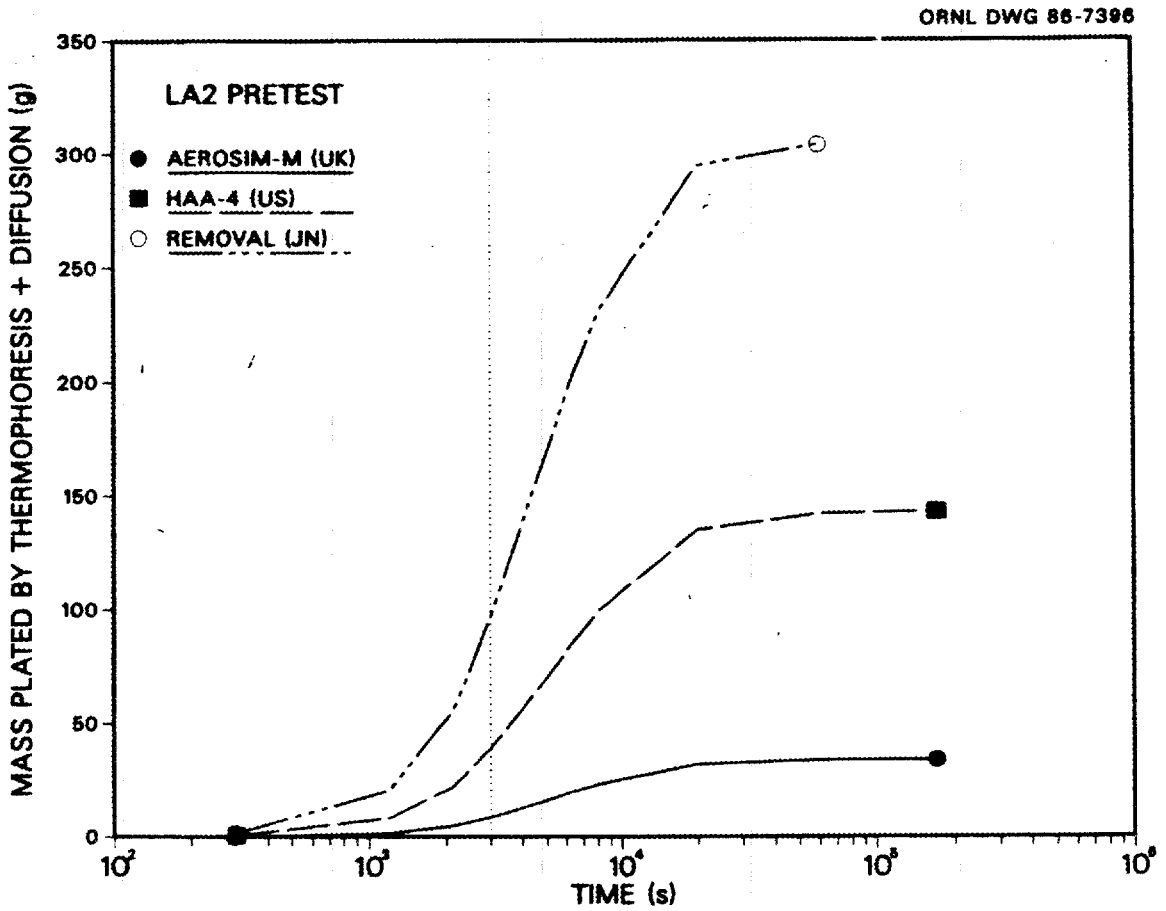

Fig. 10. LA2 pretest calculations — cumulative mass of aerosol plated in CSTF vessel by thermophoresis + diffusion vs time.

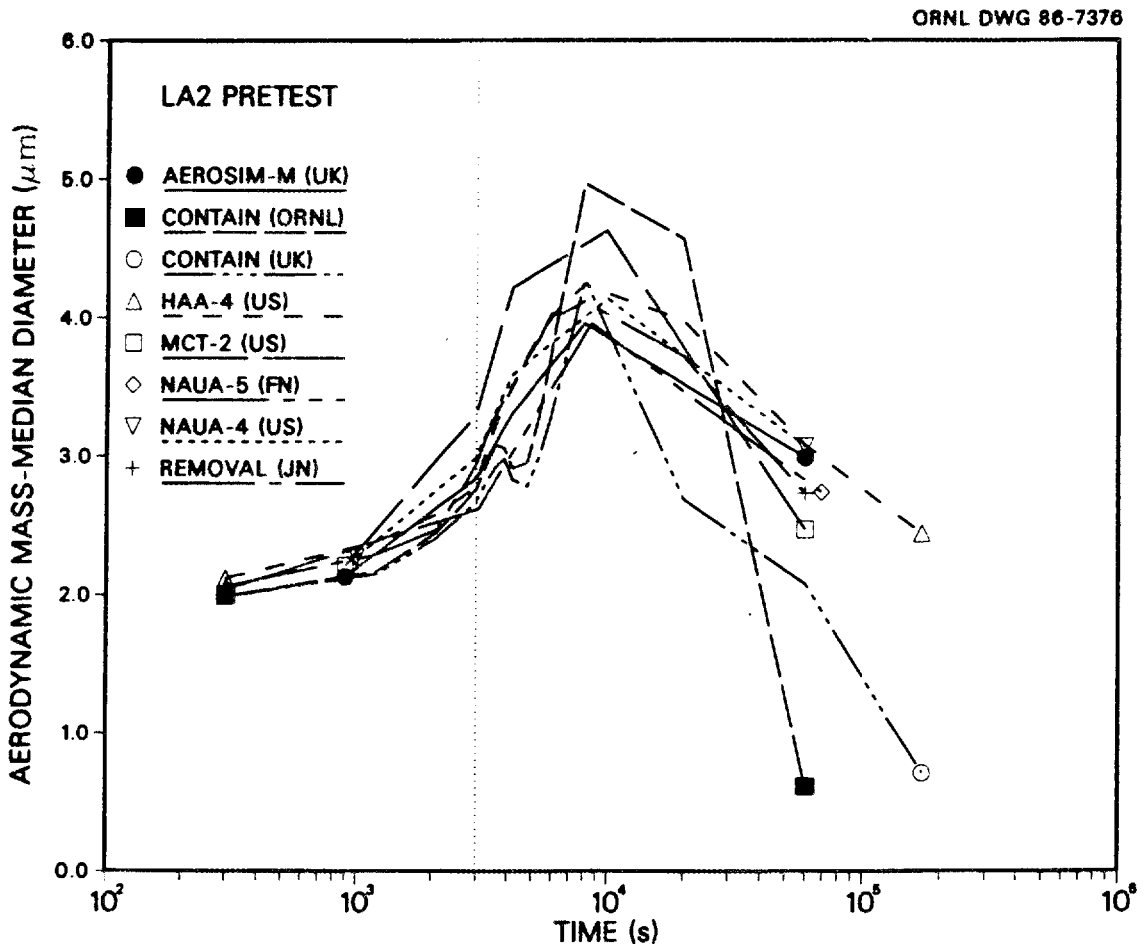

Fig. 11. LA2 pretest calculations — aerodynamic mass median diameter vs time.

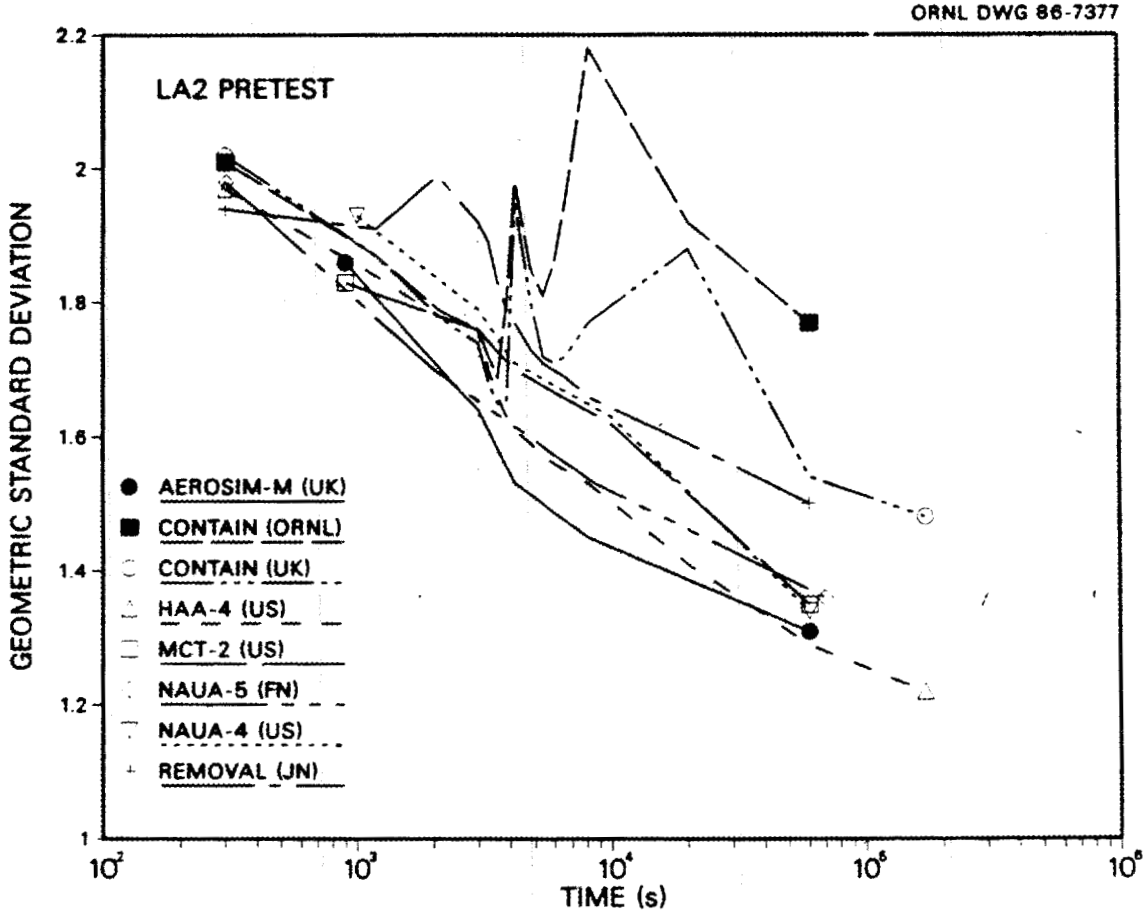

Fig. 12. LA2 pretest calculations — geometric standard deviation vs time.

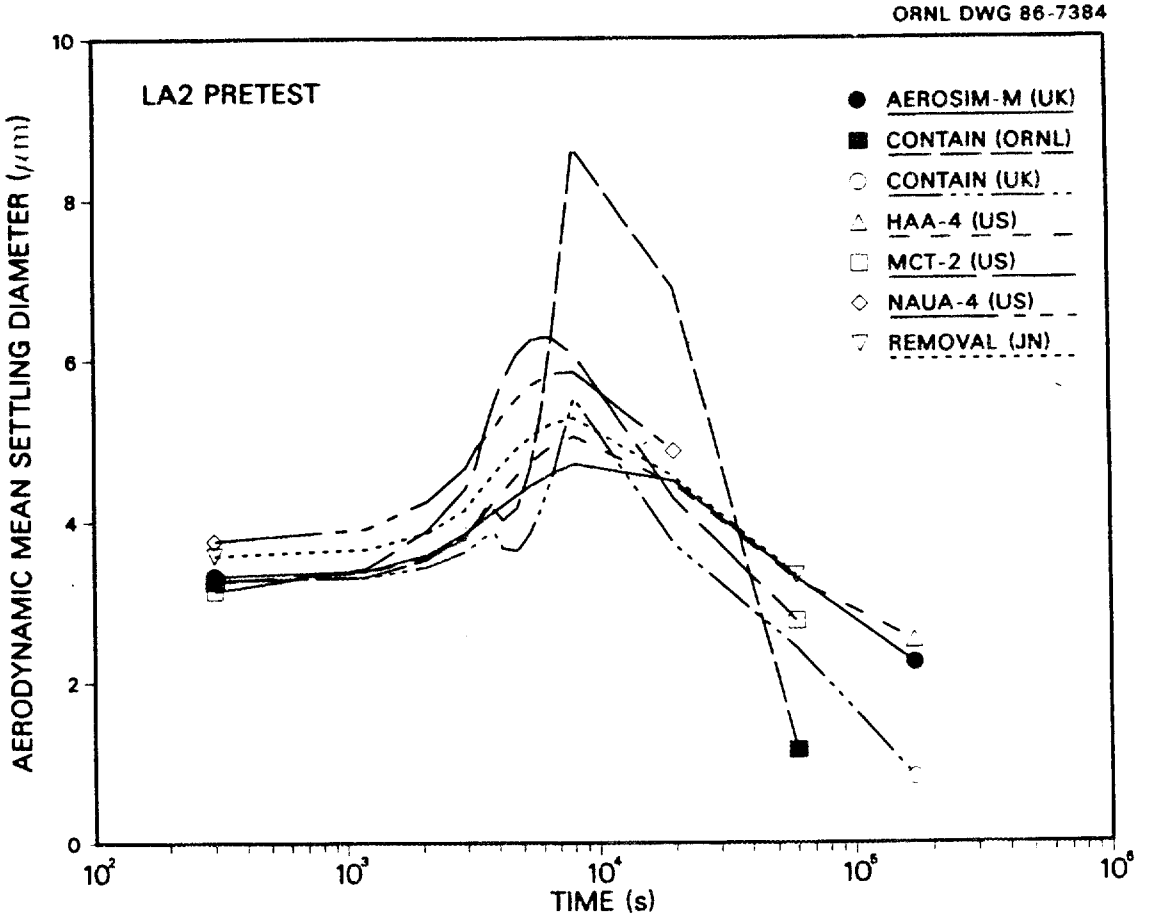

Fig. 13. LA2 pretest calculations — aerodynamic mean settling diameter vs time.

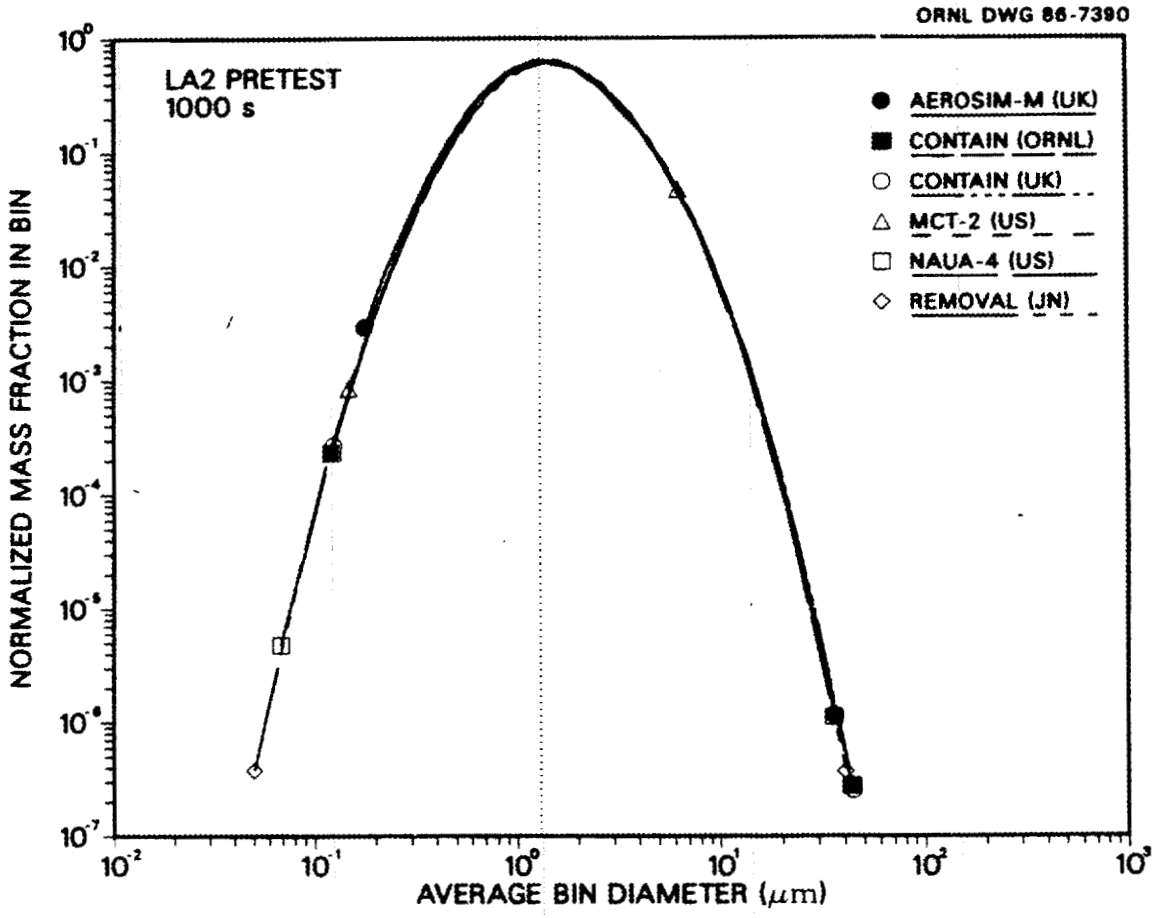

Fig. 14. LA2 pretest calculations — particle size distribution of airborne aerosol at 1,000 s.

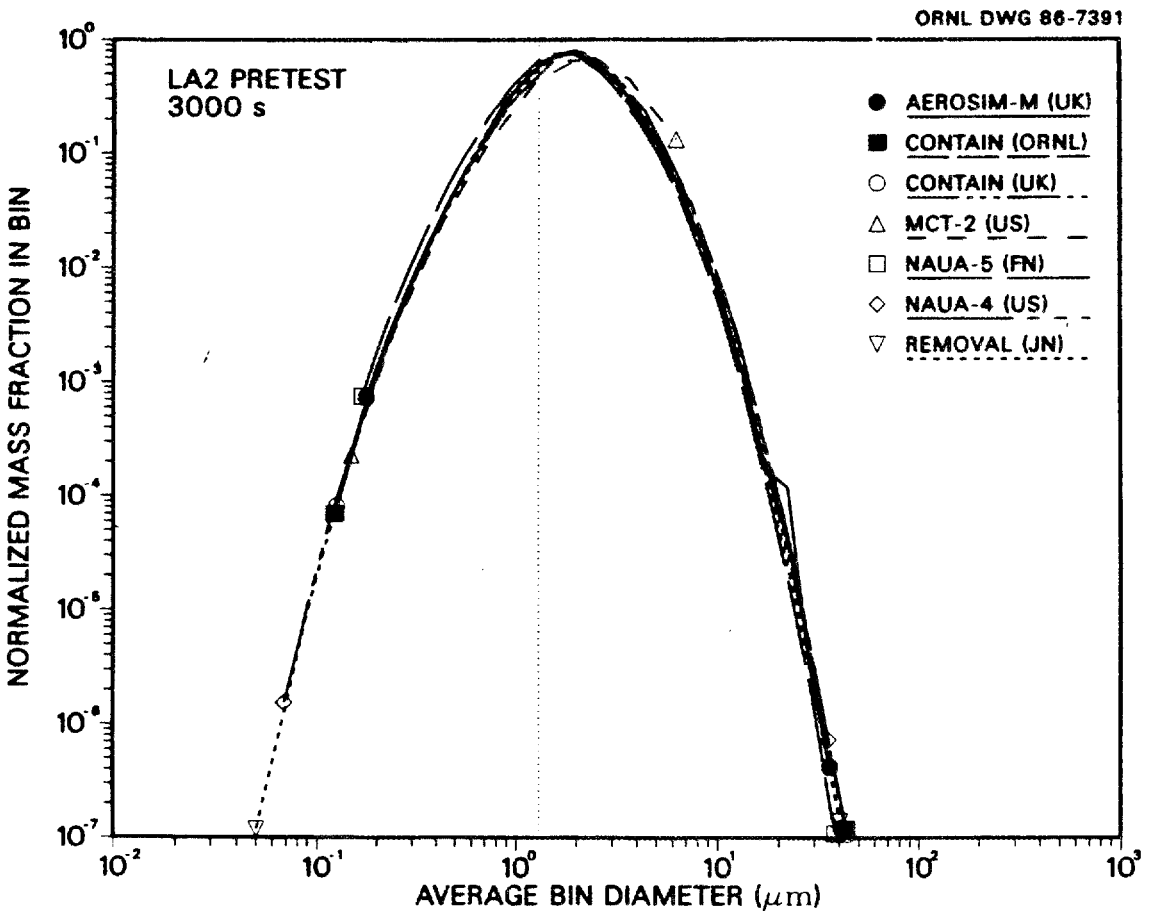

Fig. 15. LA2 pretest calculations — particle size distribution of airborne aerosol at 3,000 s.

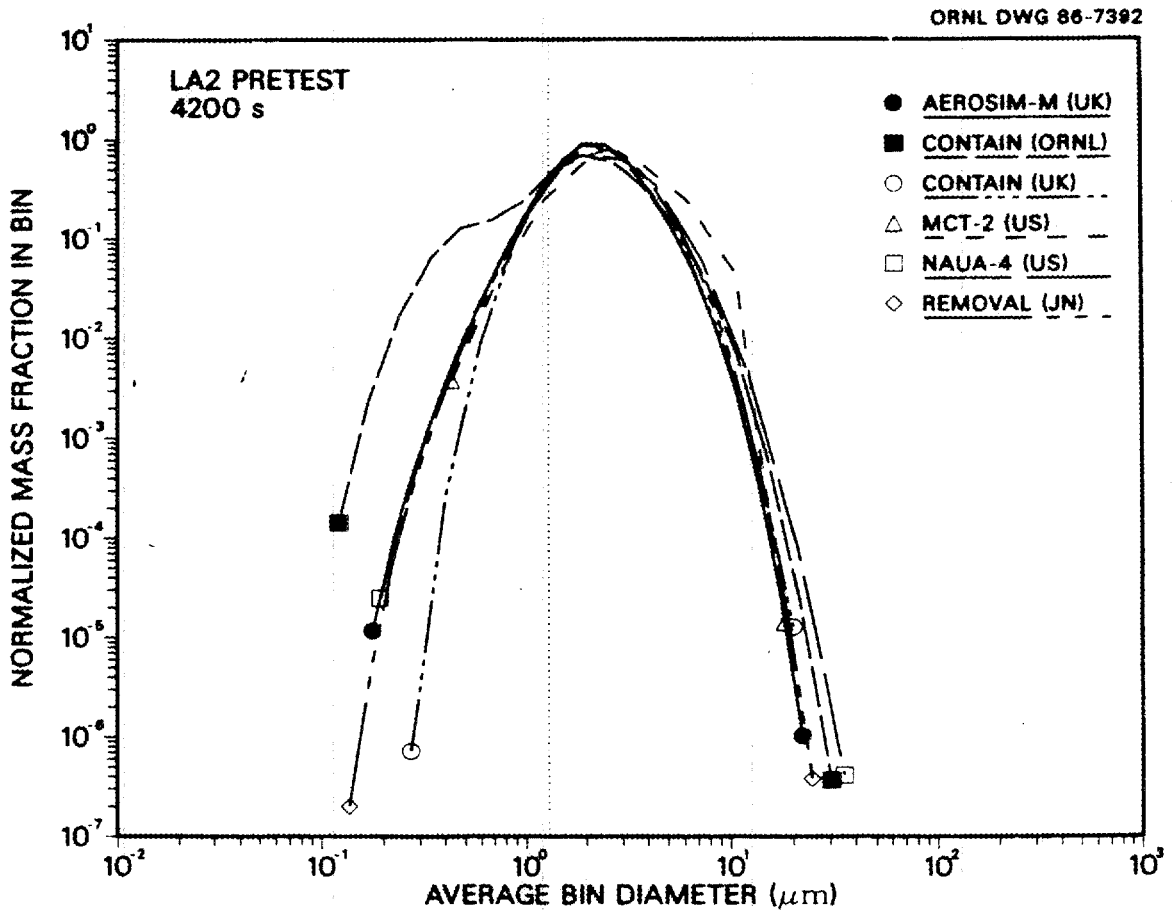

Fig. 16. LA2 pretest calculations — particle size distribution of airborne aerosol at 4,200 s.

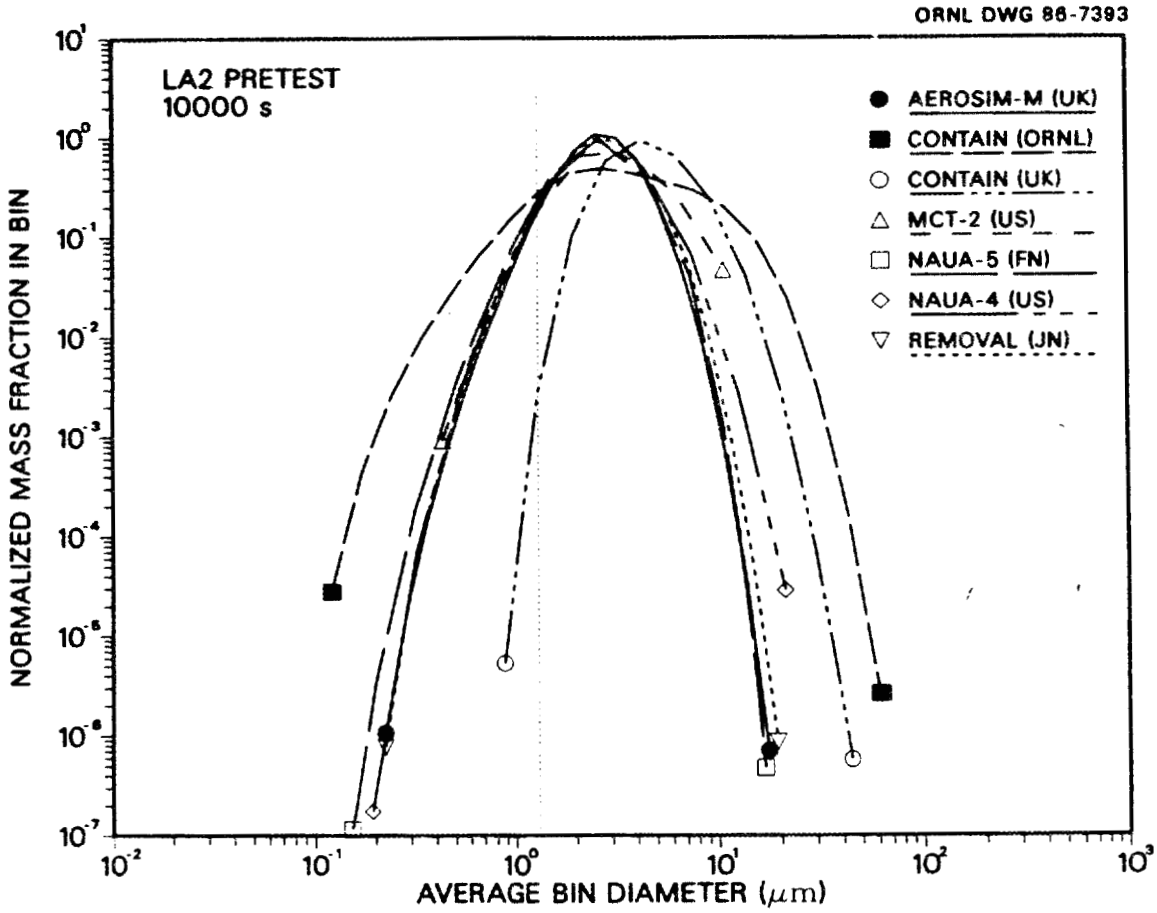

Fig. 17. LA2 pretest calculations — particle size distribution of airborne aerosol at 10,000 s.

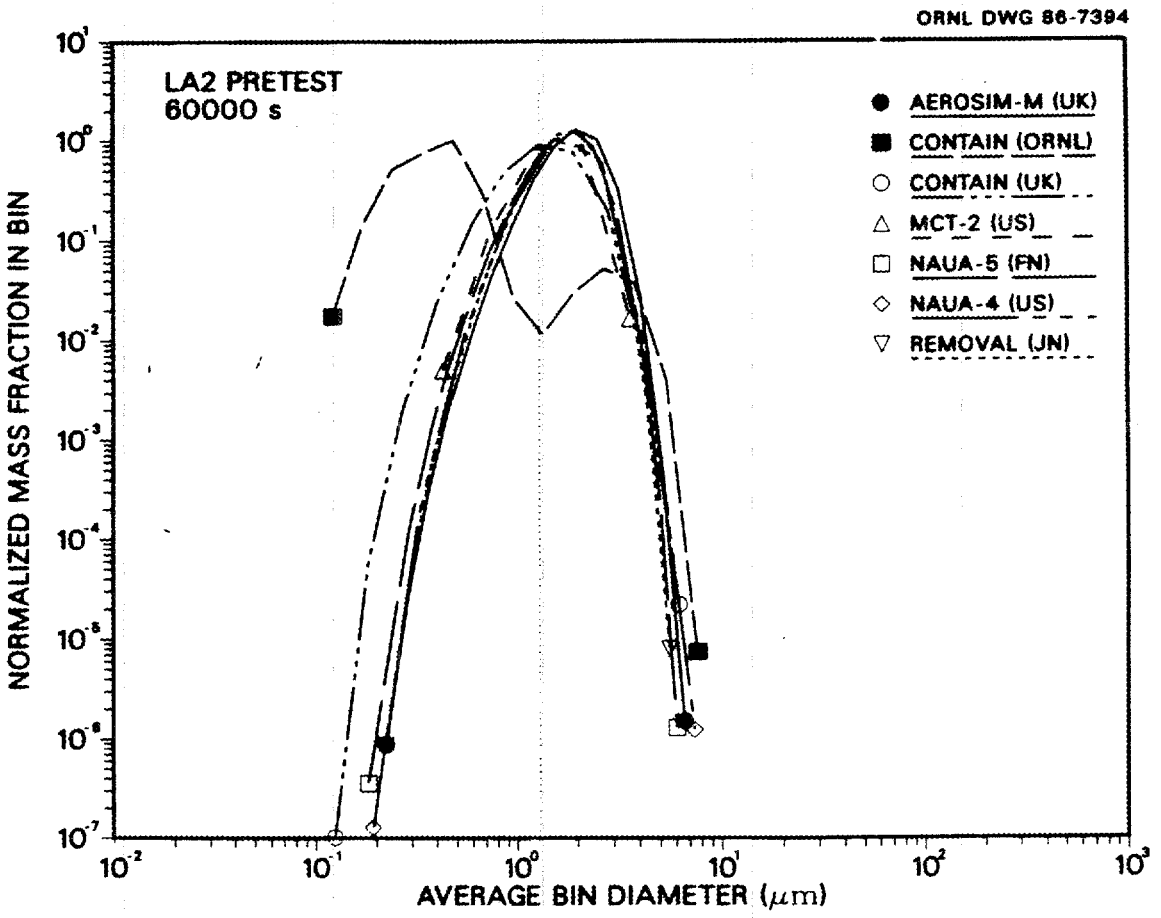

Fig. 18. LA2 pretest calculations — particle size distribution of airborne aerosol at 60,000 s.

In Figs. 19 through 21, particle size distributions for the CONTAIN (ORNL) codes are shown for times when significant amounts of water are condensed on the aerosol. In each figure, one curve is that for the wet aerosol [as was also the case for the CONTAIN(ORNL) code in Figs. 14 through 18]. This wet aerosol curve corresponds to the actual particle size distribution of the aerosol as it exists in the CSTF vessel.

Also plotted in Figs. 19 through 21 is the normalized mass fraction of the dry aerosol vs the actual diameter of the wet aerosol, as was the case for the CONTAIN(UK) code curves in Figs. 14 through 18. The values of this curve represent the particle size distribution that will be measured experimentally in LACE test LA2 by the cascade impactors, and it is this curve that will be compared with experimental results in the LA2 posttest code comparison. The cascade impactors separate the aerosol according to the actual particle aerodynamic diameters, but the mass of aerosol collected on each impactor stage is a dry aerosol mass, since any water present has been evaporated before analysis.

The third curve in each of Figs. 19 through 21 shows the normalized mass fraction of dry aerosol plotted vs the diameter of the dry aerosol. This diameter of the dry aerosol was estimated by multiplying the average diameter of each size bin by a factor, f, where

$$f = (W_d/W_w)^{1/3},$$

in which W_d is the weight of dry aerosol and W_w is the weight of wet aerosol in each bin. In deriving this conversion factor, the density of water was considered to be equal to the average density of the dry aerosol, which is the assumption used in the CONTAIN code. The CONTAIN code is not set up to handle varying densities of aerosol components.

In Figs. 22 through 24, the MnO/CsOH mass ratio in a size bin is plotted vs the average bin diameter for the particle size distributions from the AEROSIM-M and the CONTAIN codes. In these figures, the curves for both the ORNL and UK versions of the CONTAIN codes are plotted vs the diameter of the wet aerosol. As pointed out previously, the AEROSIM-M code did not predict condensation of steam on the aerosol.

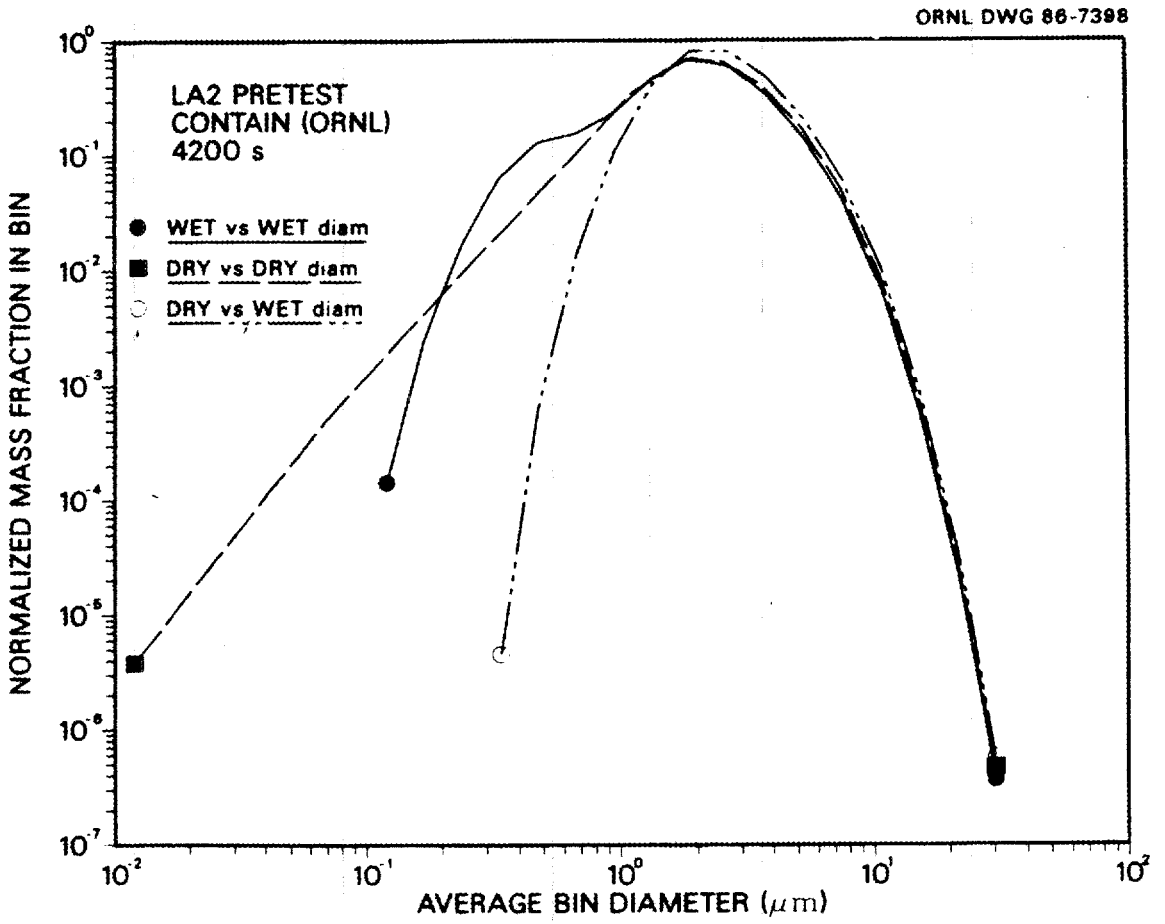

Fig. 19. LA2 pretest calculations — particle size distributions of airborne aerosol at 4,200 s for the CONTAIN(ORNL) code.

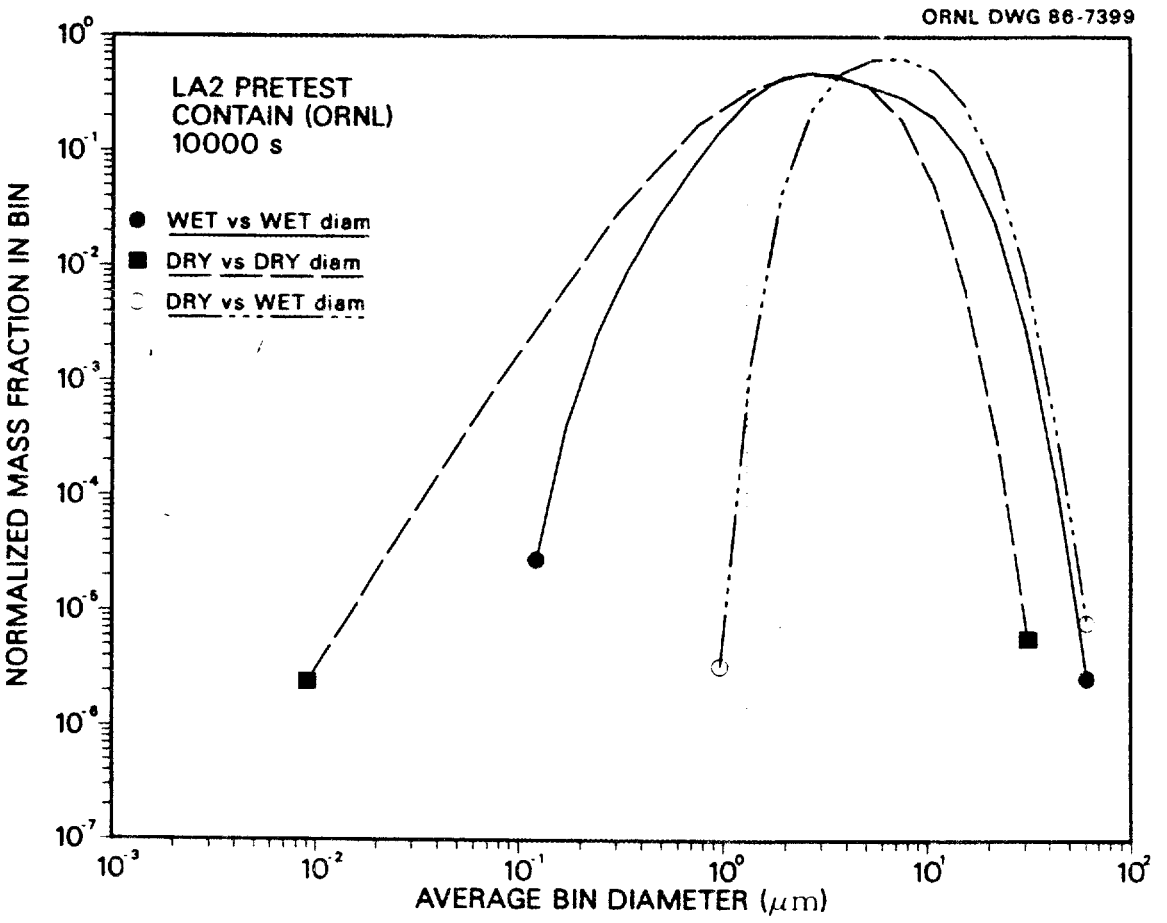

Fig. 20. LA2 pretest calculations — particle size distributions of airborne aerosol at 10,000 s for CONTAIN(ORNL) code.

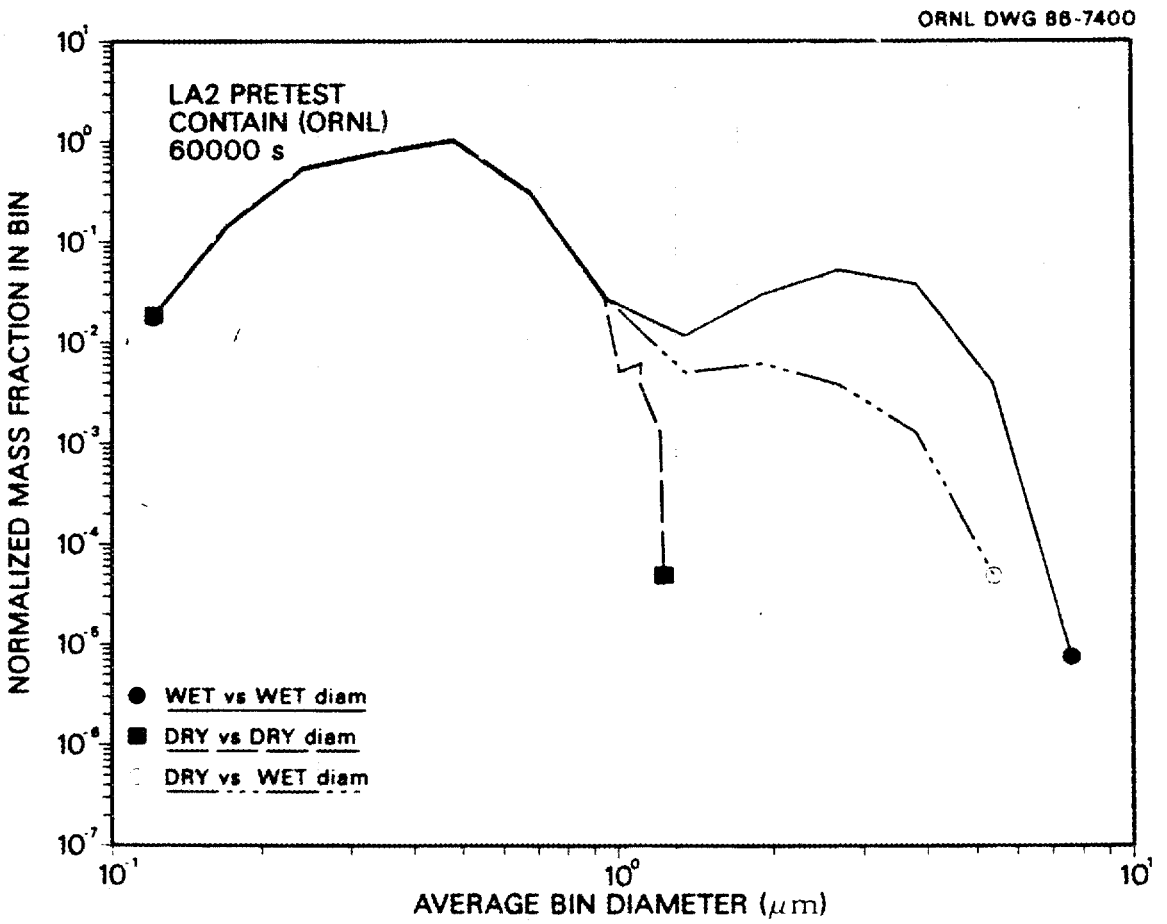

Fig. 21. LA2 pretest calculations — particle size distributions of airborne aerosol at 60,000 s for CONTAIN(ORNL) code.

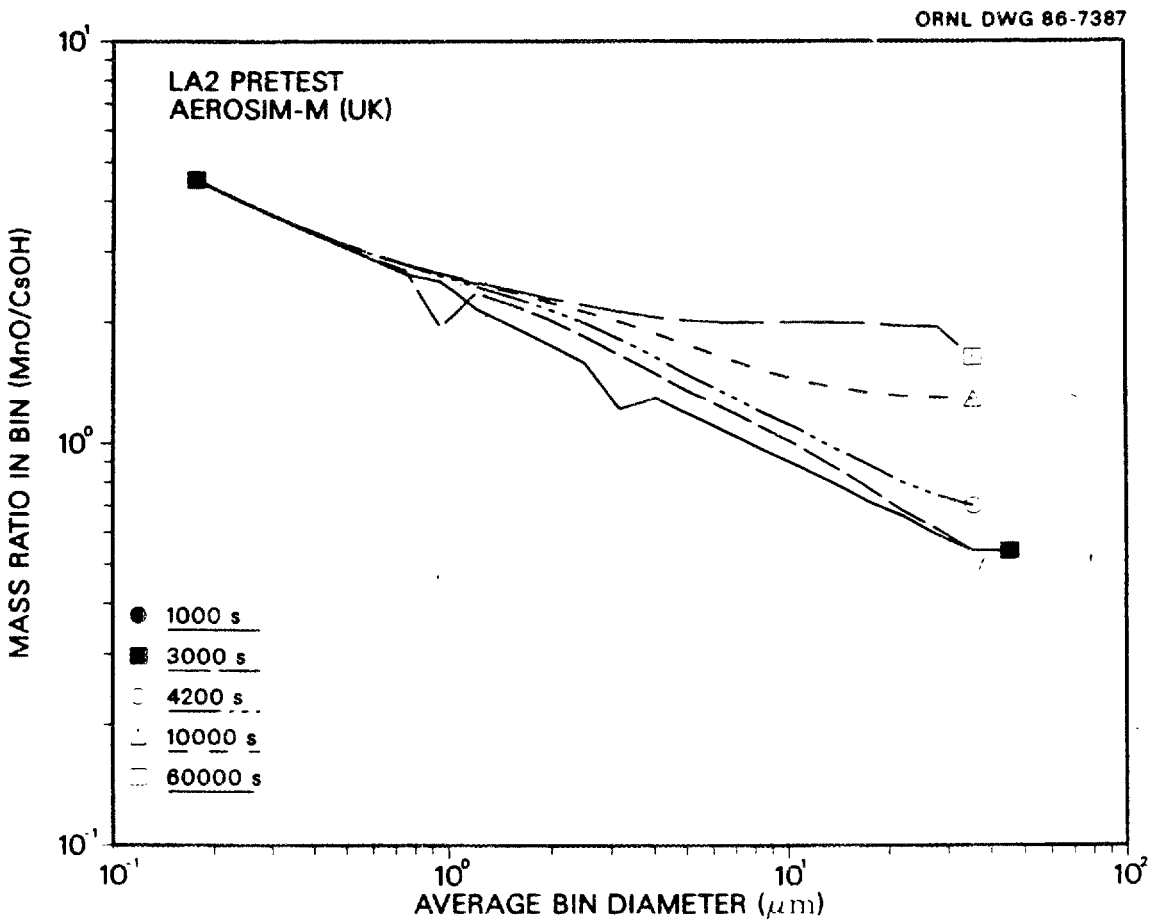

Fig. 22. LA2 pretest calculations by the AEROSIM-M code — MnO/CsOH mass ratio vs bin diameter for airborne aerosol particle size distribution.

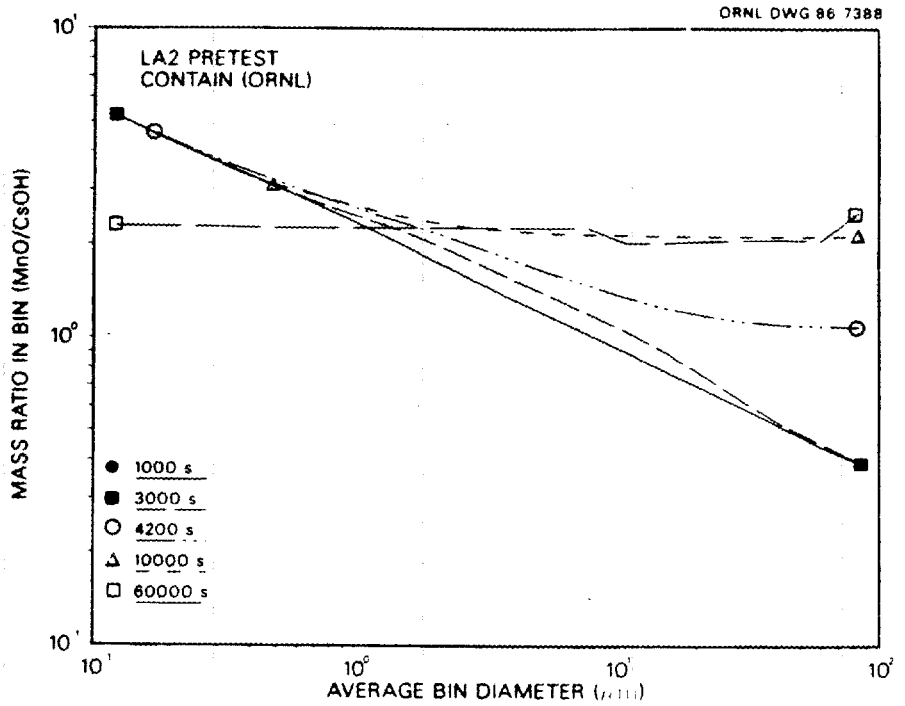

Fig. 23. LA2 pretest calculations by the CONTAIN(ORNL) code — MnO/CsOH mass ratio vs bin diameter for airborne aerosol particle size distribution.

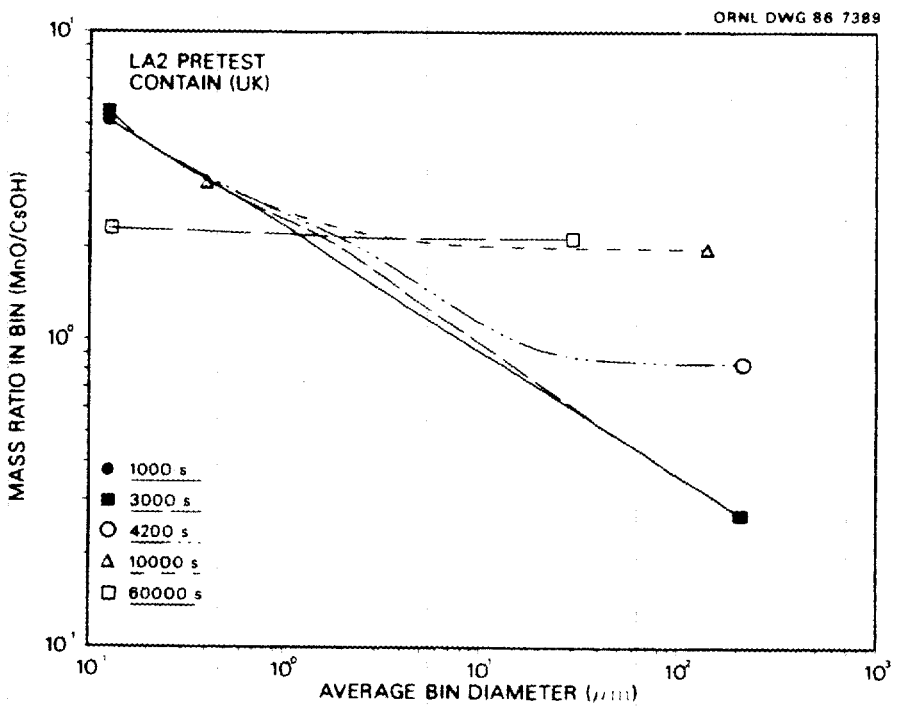

Fig. 24. LA2 pretest calculations by the CONTAIN(UK) code — MnO/CsOH mass ratio vs bin diameter for airborne aerosol particle size distribution.

The MnO/CsOH mass ratios for the airborne aerosol and for the cumulative settled aerosol are plotted vs time in Fig. 25. The AEROSIM-M and the CONTAIN codes provided this type of information. The mass ratio for the cumulative plated aerosol was essentially constant with time at a value of ~2. The instantaneous mass ratio for the leaked aerosol would be equal to that for the airborne aerosol.

4. GENERAL COMMENTS ON LA2 PRETEST CALCULATIONS

In the LA2 pretest instruction letter,[2] the mixed aerosol source was specified as having an AMMD of 2 μm and a GSD of 2 for calculation purposes. For the multicomponent codes, the mass-median diameters were provided for MnO and CsOH. These diameters were calculated assuming that each source species also had an AMMD of 2 μm. Since the instruction letter did not specify the GSD for the separate MnO and CsOH source aerosols, all code analysts assumed the GSD to be 2 for each. While this ambiguity in the instruction letter did not cause a problem here, all particle size distribution parameters should be provided in future specifications for aerosol calculations. When specifying input for a single-component aerosol code, the particle size distribution parameters for a mixed-source aerosol should be determined by an appropriate method (for example, by combining the values for separate aerosol species on a lognormal probability distribution plot).

Some of the AMMD results of the "discrete" codes appeared anomalous, in that at early times during the aerosol generation period the AMMD values differed from the AMMD of the source. At these early times, the AMMD of the source should be reproduced (assuming no water is condensed on the aerosol). By definition the mass-median diameter, which is used to calculate the AMMD, is that diameter below which 50% of the mass of the particle size distribution lies. In order to facilitate comparisons with experimental impactor data, the codes should calculate the AMMD in a manner consistent with this definition. For example, the mass-median diameter may be determined from "discrete" code data by plotting cumulative mass vs the upper diameter of the size bin, since the diameter of all the particles in that bin is smaller than or equal to the upper bin

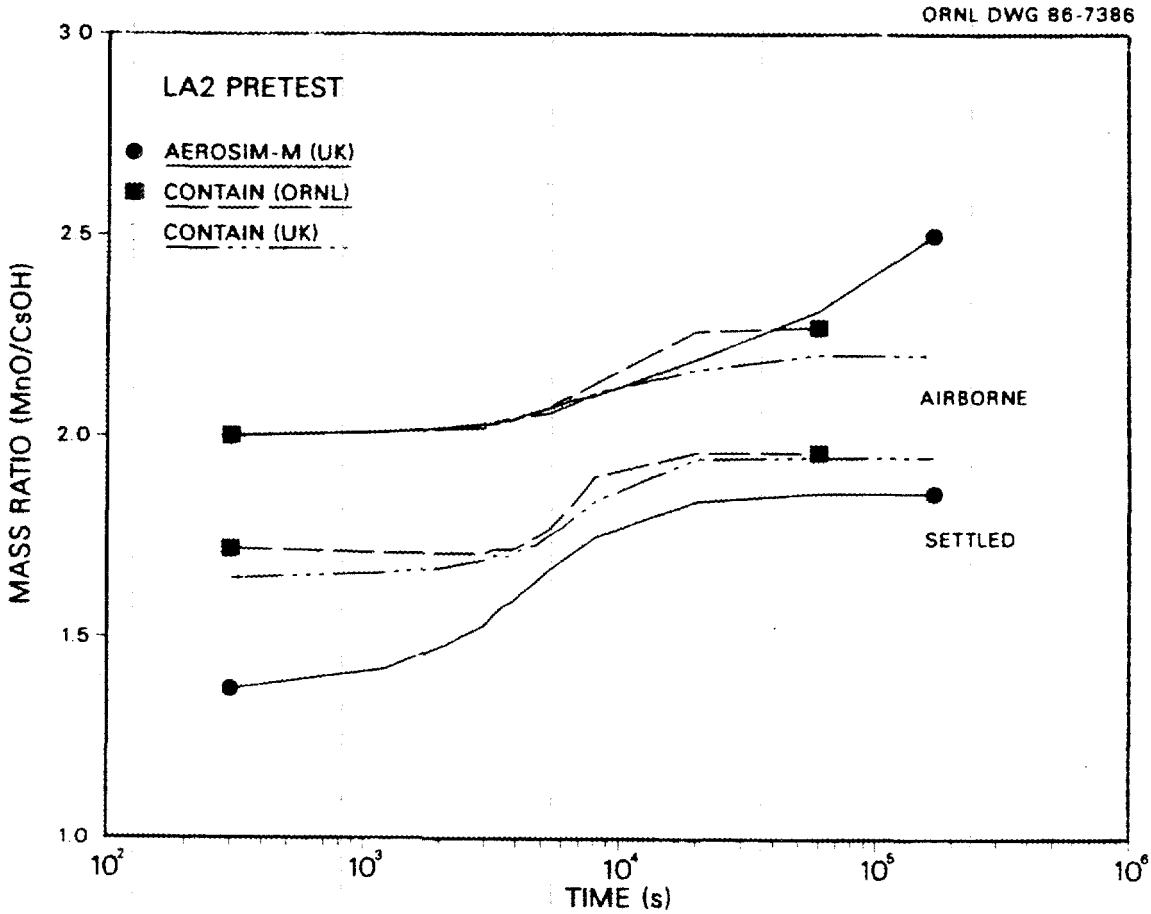

Fig. 25. LA2 pretest calculations — MnO/CsOH mass ratio in cumulative settled aerosol and in total airborne aerosol vs time.

diameter. The problem is that some codes utilize the average rather than the upper bin diameter when determining the mass-median diameter by this approach. Another problem is that some codes use a formula for the mass-median diameter which applies only to a lognormal distribution. We calculated AMMD values using the reported particle size distribution data. Significant differences were found between our values and those reported by several codes. The code users were notified of these findings so that they could reevaluate their methods of determining AMMD. Wherever applicable, the AMMD values presented in the next section include our values calculated using the particle size distribution data reported by the codes.

As mentioned in the previous section, the particle size distribution curves presented here have been normalized to represent probability density functions. To illustrate the desirability of this, consider a particular distribution curve and then increase the number of bins by a factor of 10, while keeping the maximum and minimum particle diameters constant. The mass fraction in a size bin at any bin diameter would then be reduced by about a factor of 10. If the mass fraction in each bin were plotted vs bin diameter for both these cases, two similar curves would be generated that would be displaced vertically from each other. However, if normalization is performed, the two curves would coincide — as they should, since they represent the same particle size distribution. This is illustrated in Fig. 14, where the particle size distributions for all codes are, and should be, approximately the same as that of the source at the early time of 1,000 s.

In analyzing the LA2 pretest results, the aerodynamic mean settling diameters reported by the codes could not be verified (mainly because viscosities of the CSTF atmosphere and settling rates were not available in all cases). However, using estimated viscosities and settling rates where necessary, we calculated settling diameters. For some codes, the differences between our calculated and the reported settling diameters were greater than would be expected due to any differences in the viscosities and settling rates used by us and by the code. More information about the codes is needed to determine the reason for these differences

in settling diameter calculations. The use of such a parameter as the settling diameter for code-comparison purposes is seen to have potential problems. Although this parameter is not used elsewhere in the code calculations, possible errors or differences in calculation methods for the parameter may lead one to suspect significant differences between codes which, in fact, do not exist. The AMMD is another example of such a parameter.

The CONTAIN code is an integrated code, combining both the thermal-hydraulic and aerosol-behavior calculations. For the LA2 pretest calculations, the CONTAIN(ORNL) code predicted time histories for the vessel leak rate and the rate of steam condensation on vessel surfaces that differed from the values specified in the LACE instruction letter (the instruction letter gave estimates of expected experimental results; actual test measurements provided significantly different data).[2] This information was not provided by the code users for the CONTAIN(UK) code. Futhermore, both codes predicted condensation of steam on the aerosol particles. Thus, the results of these two versions of the CONTAIN code are difficult to compare (not only to the results of the "dry" codes, but also to each other) because (1) the leak rate directly affects the airborne aerosol concentration, (2) the steam condensation rate on surfaces is used in the calculation of diffusiophoresis, and (3) condensation on the aerosol affects the settling rate. Simulation of actual thermal-hydraulic conditions is also a potential problem for the CONTAIN codes in the blind posttest aerosol calculations.

In the LA2 test plan[1] and the LA2 pretest instruction letter,[2] surface areas were specified for plateout, settling, and heat transfer. Table 5 shows that three different values for area were used by the three codes that provided separate values for plating by thermophoresis. The areas used were either the plateout area, the heat transfer area, or an area intermediate to these two. When the instruction letter was prepared, it was not recognized that there would be any ambiguity in selecting the area for the thermophoresis mechanism. Specifications for future LACE calculations should carefully avoid any ambiguities that can affect the code comparison efforts.

5. DISCUSSION OF RESULTS OF LA2 PRETEST CALCULATIONS

Airborne aerosol concentration

As seen in Figs. 1 through 3, the airborne aerosol concentration values during the aerosol generation period showed good agreement for all codes except the NAUA-5 code. For this time period, the leak-rate input to the NAUA-5 code was ~10 times too high, which resulted in low concentration values. After termination of the source aerosol generation, the concentration values for the NAUA-5 code do not decrease as rapidly as do those for the other codes. This is probably because the NAUA-5 code includes only plating by Brownian diffusion, which does not produce significant deposition.

Beginning at time 3,000 s, the MAAP-2.9 code predicts a rapid drop in aerosol concentration. The MAAP-2.9 aerosol concentration values are lower than those for the other codes, except at approximately 12,000 and 28,000 s when the CONTAIN(ORNL) and REMOVAL codes, respectively, predict lower concentrations. The initial rapid drop after 3,000 s is the result of high deposition rates during this time period. As seen in Fig. 5, ~85% of the total cumulative deposition occurred by ~5,000 s. The reason for the relatively slower concentration decrease at longer times could be the fact that MAAP-2.9 assumes the aerosol to have an asymptotic particle size distribution independent of the source particle size.[4] If the asymptotic particle size is significantly less than the average size predicted by the other codes at the same aerosol concentration, then MAAP-2.9 calculated values may show a slower rate of concentration decrease at the later times.

The CONTAIN(ORNL) code predicts a rapid drop in aerosol concentration after termination of the source aerosol. This is believed to be a result of the code's calculation of water condensation on the aerosol. As seen in Fig. 4, water evaporation is not predicted to begin until ~30,000 s. The CONTAIN(UK) code predicts evaporation to begin at ~10,000 s. Consequently, the aerosol concentration behavior predicted by the CONTAIN(UK) code differs from that predicted by the CONTAIN(ORNL) code.

Aerosol leakage and deposition

From Figs. 5 and 6, it is evident that the NAUA-5 code predicts a low mass of aerosol retained and a corresponding high amount of aerosol leaked. As discussed previously, the code assumed a leak rate that was too high (by a factor of ~10) during aerosol generation. Also, the MAAP-2.9 code calculated high deposition rates that resulted in a high value for the retained aerosol mass, as seen in Fig. 5. The MAAP-2.9 calculation used a collision shape factor of 2.5 (instead of 1, as specified in the pretest instruction letter[2]). The high deposition rates most likely were caused by the high value of this shape factor. The amounts of retained mass calculated by the two CONTAIN codes are believed to be higher values than those for the five remaining codes, because CONTAIN includes the influence of steam condensation on aerosol settling. This is demonstrated in Fig. 7, which shows that the rate of aerosol settling predicted by the CONTAIN codes increases near the onset of steam condensation. Based on the high amount of retained mass, the airborne aerosol concentration predicted by the CONTAIN(UK) code appears to remain unusually high at the longer times, as seen in Fig. 1. Figure 11 shows that the probable reason for this is the relatively low value of the AMMD that results after the evaporation of water.

Figures 3 and 5 indicate that the airborne aerosol concentration values at later times are inversely related to the values for aerosol mass retained (by settling and plating) for the AEROSIM-M, HAA-4, MCT-2, NAUA-4, and REMOVAL codes. If there are no confounding factors* (such as differences in volumetric leak rates utilized by the codes), such a relationship would be expected. Figure 7 shows that values for the cumulative settled aerosol masses calculated by three of these codes, AEROSIM-M, NAUA-4, and REMOVAL, agreed reasonably well (MCT-2 did not report separate values for settling and plating). The settled mass value for the HAA-4 code was somewhat higher. Thus, some of the differences in predicted concentration behavior appear to be related to plating estimations.

---

*Such factors could not be assessed, because requested copies of code input were not provided by all code users.

For the AEROSIM-M, NAUA-4, and REMOVAL codes, which predicted similar settling behaviors, Fig. 8 indicates that plating differences contributed to differences in the airborne concentration behavior at later times. Although the HAA-4 code predicted a lower plated mass than did AEROSIM-M, the higher settled mass of HAA-4 resulted in the same retained mass value as AEROSIM-M (shown in Fig. 5) and, consequently, HAA-4 predicted a concentration behavior similar to that of AEROSIM-M. Figures 9 and 10 illustrate the differences in plating predictions.

In Fig. 9, the REMOVAL and the NAUA-4 codes show the highest plating values for the diffusiophoresis mechanism. The AEROSIM-M code gives an intermediate value, and the HAA-4 code the lowest value for diffusiophoretic plating. If the four codes utilized the steam condensation rate specified in the instruction letter[2] (again, this could not be ascertained because of the lack of information provided), there must be basic differences in the diffusiophoresis models used by these codes.

Figure 10, shows that REMOVAL had the highest value for plating due to thermophoresis and Brownian diffusion, with HAA-4 and AEROSIM-M having succeedingly lower values. The predicted Brownian diffusion plating values were insignificant for the REMOVAL and HAA-4 codes, and this is assumed to be true also for AEROSIM-M. The NAUA-4 code did not include the thermophoresis mechanism, and the predicted amount of Brownian diffusion plating was negligible. For thermophoresis calculations, the instruction letter[2] specified a temperature difference of 4 K. For the temperature gradient, the REMOVAL, HAA-4, and AEROSIM-M codes used thermal boundary-layer thicknesses of 2, 3, and 10 mm, respectively, as shown in Table 5. Also, these codes used different values for the plating area. The thermophoretic plating value, when adjusted to the same basis as that of REMOVAL, is ~240 g for both the AEROSIM-M and HAA-4 codes. The plating value for REMOVAL was 300 g. Thus, possible differences in the thermophoresis models of these codes are indicated.

For the CONTAIN codes, the high values for settled aerosol mass (Fig. 7) are a result of the predicted condensation on the aerosol which causes an increase in settling rates. If most of the plating can be

assumed to be due to diffusiophoresis for the CONTAIN codes, then Figs. 8 and 9 indicate that the diffusiophoresis plating values for CONTAIN(ORNL) and CONTAIN(UK) are somewhat less and somewhat higher, respectively, than that for AEROSIM-M. Since the CONTAIN code is integrated, it calculates the thermal-hydraulic behavior rather than using the specifications in the instruction letter. However, the predicted steam condensation rate could not be determined from the computer output provided for CONTAIN (ORNL) nor was it reported for CONTAIN(UK). Consequently, the plating results for the CONTAIN codes could not be evaluated.

Using an average aerosol concentration curve (generated by averaging the logarithms of the concentrations in Fig. 1) and the thermal-hydraulic information supplied in the instruction letter,[2] the mass of aerosol plated by diffusiophoresis can be calculated by a representative model. Thus, the rate of aerosol deposition by diffusiophoresis, R_a, is related to the steam condensation rate, R_s, by

$$R_a = R_s\ C_a/\{\rho_s[1 + (F_g/F_s)\cdot(M_g/M_s)^{0.5}]\},$$

where C_a and ρ_s are the aerosol concentration and the steam concentration, respectively, in g/m^3; F_g and F_s are the gas and steam mole fractions, respectively; and M_g and M_s are the gas and steam molecular weights, respectively.[5] By integrating this expression over time, the calculated aerosol plating by diffusiophoresis is 590 g. This agrees with the result from the AEROSIM-M code seen in Fig. 9.

A discrepancy between the above equation and that used by the NAUA-4 code for plating by diffusiophoresis was discovered after the first draft of this report was issued.[6] The NAUA-4 code divides the above equation by the mole fraction of steam (this explains the difference between the value of 590 g, calculated using the above equation, and the amount of 1047 g predicted by NAUA-4 in Fig. 9). We have found that the NAUA-4 equation was based on an error in the original paper.[7] A copy of the user's manual for REMOVAL/MODO that was received showed also that the REMOVAL equation for plating by diffusiophoresis is identical to that of NAUA-4, which explains the good agreement between these two codes shown in Fig. 9.

Aerosol particle size distribution parameters

Figures 11 through 13 illustrate how the particle size and the particle size distribution of the suspended aerosols vary with time. Soon after the initiation of aerosol injection, the AMMD and the GSD are approximately the same as those of the source aerosol, as expected when little or no water is condensed on the aerosol. All of the "dry" (no steam condensation onto the aerosol) codes predict similar behaviors for the AMMD, the aerodynamic mean settling diameter, and the GSD. However, between the times of 1,000 and 20,000 s, the MCT-2 code predicts a somewhat higher AMMD. Also, the GSD value of the REMOVAL code is the highest of those from the "dry" codes. The AMMD values of the "dry" codes are seen to increase initially, presumably as a result of agglomeration. At later times, when low airborne aerosol concentrations result in low values of agglomeration rate, the AMMD values decrease as the result of larger particles preferentially settling out. The GSD values of the "dry" codes decrease with time. This narrowing of the particle size distribution can be explained by the growth of the smaller particles through agglomeration and the faster settling rates of the larger particles. As seen previously, the airborne aerosol concentration behavior for the NAUA-5 code was affected by an error in the input leak rate. However, the AMMD and the GSD values for NAUA-5, when compared to those of the other codes, appear not to have been significantly affected.

Figures 11 through 13 show the effects (beginning at ~4,000 s) of steam condensation on aerosol in the calculations by the CONTAIN codes. As expected, the AMMD and the settling diameter values increase fairly rapidly at the onset of condensation and then decrease with evaporation when superheated conditions occur. However, the AMMD values calculated by the CONTAIN codes decrease to significantly lower levels than those for the "dry" codes. This is not entirely unexpected, since condensation of steam on the aerosol will increase the settling rate, particularly that of the larger particles. A deagglomeration phenomenon may be partly responsible for the calculated decrease in AMMD after evaporation. This phenomenon is discussed later. The settling diameter is also predicted

by CONTAIN to be lower after evaporation, but the difference is not as pronounced. In Fig. 12, the GSD values for the CONTAIN codes are seen to increase when steam condensation begins. This may be attributed to the higher concentration of water in the lower particle size bins, as seen in Figs. 19 and 20. After evaporation of water begins, the predicted GSD for the CONTAIN(ORNL) code decreases but remains relatively high. As seen in Fig. 21, the larger particles are predicted by CONTAIN to have a significant amount of water even at 60,000 s, which results in a continuation of high GSD values.

As mentioned previously, the MCT-2 results included a "wet" case. The amount of water condensed on the aerosol was determined by a material balance method, and condensation on the aerosol was predicted to a time of ~2,100 s. The results of the MCT-2 calculations, which were carried out to 20,000 s, produced airborne aerosol concentration values which were ~25% lower than those for the "dry" case. The value for mass of aerosol retained was increased by ~14%. As expected, the AMMD values were significantly greater for the "wet" case during condensation. For later times, the AMMD for the "wet" case was <10% lower than that for the "dry" case. Because of the relatively short duration of the predicted supersaturated conditions, steam condensation on aerosol did not have a very significant effect in the MCT-2 calclulations.

The aerosol particle size distributions plotted in Figs. 14 through 18 show very good agreement between the codes at 1,000 s and 3,000 s. At 4,200 s, the distributions of the "dry" codes begin to show some differentiation at the larger particle sizes. Despite the NAUA-5 code error in the input leak rate, the particle size distributions calculated by this code were very similar to those of the other "dry" codes. At 4,200 s, the CONTAIN(ORNL) code shows an increase in the normalized mass fraction values in the smaller size bins. This results from the greater amounts of condensed water predicted for these smaller size bins. The CONTAIN(UK) code shows a shift of the left hand side of the distribution to larger particle sizes due to the growth of the smaller particles into larger size bins as a result of steam condensation. The curve for CONTAIN(UK) represents the distribution of the dry aerosol vs the actual size of the

wet aerosol, as information on the amount of water associated with each size bin was not provided. If the distribution of the wet aerosol were plotted, it probably would be similar to that for the CONTAIN(ORNL) code.

At 10,000 s and at 60,000 s, good agreement continues between the distribution values for the "dry" codes. The effect of steam condensation on the aerosol in the CONTAIN(UK) code is very evident at 10,000 s as the entire distribution curve for the dry aerosol has been shifted toward larger particle sizes. The CONTAIN(ORNL) distribution curve for the wet aerosol at 10,000 s is very broad, due to the prediction of significant water in all size bins. Growth into the larger size bins as a result of steam condensation causes an increase in estimated settling rates and the larger values for AMMDs and settling diameters that were mentioned previously for the CONTAIN codes. Under superheated conditions at 60,000 s, the CONTAIN(UK) code predicts a shift to smaller sizes at the lower end of the distribution than those predicted by the "dry" codes. For the CONTAIN(ORNL) code, the effect is much more dramatic; Fig. 18 shows the shift to high concentrations of the smaller particles, and the distribution has a bimodal appearance as well. A shift to smaller particle sizes is expected as a result of evaporation (since the diameter of the dry aerosol is less than that of the wet aerosol). However, the relatively high concentrations of very small particles, particularly those predicted by the CONTAIN(ORNL) code, appear unusual. This is believed to be a result of the deagglomeration phenomena discussed in the next subsection.

In Figs. 19 and 20, the CONTAIN(ORNL) curves for normalized mass fraction of dry aerosol vs wet aerosol diameter are seen to be very similar to those for the CONTAIN(UK) code in Figs. 16 and 17. An analysis of Figs. 19 and 20 indicates that the condensed water is concentrated in the lower size bins at 4,200 s, while at 10,000 s all size bins contain appreciable amounts of water. Consequently, if the water were evaporated, one would predict that both the lower part of the "dry vs wet diam." curve in Fig. 19 and the entire "dry vs wet diam." curve in Fig. 20 would shift toward smaller particle sizes. The "dry vs dry diam." curves in Figs. 19 and 20 confirm this prediction. However, aerosol particles with diameters smaller than even the smallest size bin used in the

CONTAIN(ORNL) calculation are seen to be generated. This suggests that deagglomeration of the aerosol has somehow occurred.

In Fig. 21, the condensed water is predicted by the CONTAIN(ORNL) code to be concentrated in the larger particle sizes at 60,000 s. This causes the bimodal shape of the two curves plotted vs the wet aerosol diameter. If the water were evaporated, the actual diameters of the resultant dry aerosol particles should be smaller than predicted by the two wet aerosol curves plotted in Fig. 21, especially at the larger particle sizes. The "dry vs dry diam." curve in Fig. 21 demonstrates this. The mass-median diameter of the dry aerosol appears to be ~0.5 μm, compared to 1.31 μm for the mixed-source aerosol.

In Fig. 22, which shows the variation in composition of the particle size distribution with bin size, at times of 900 s and 3,000 s the AEROSIM-M code predicts a decrease in the MnO/CsOH mass ratio as the average bin diameter increases. Since the MnO/CsOH mass ratio of the source is 2.0, and the MnO aerosol has the smaller particle size distribution, this is to be expected at these early times. At longer times, the agglomeration of particles with different MnO/CsOH mass ratios causes the mass ratio in the bins >5 μm to approach a value slightly >2.0. The mass ratio for the smaller size bins is not affected because particles are always removed from rather than added to the smaller bins by agglomeration.

The CONTAIN codes also predict that the MnO/CsOH mass ratio will decrease with increasing particle diameter at early times (see Figs. 23 and 24). However, at 60,000 s the mass ratio is predicted to be essentially constant for all bin diameters, rather than just for the larger size bins (as predicted by the AEROSIM-M code). This implies that some of the larger particles with a low MnO/CsOH mass ratio must somehow experience a significant reduction in size and mix with the smaller particles. This does not seem physically possible, nor does the CONTAIN code specifically include such a mechanism. Again, this is believed to be due to the deagglomeration phenomenon. For both the CONTAIN and the AEROSIM-M codes, the mass ratio actually should approach a constant value

for the larger size bins, as shown in Figs. 23 and 24 at 10,000 s. Since the curves at 10,000 s represent the MnO/CsOH mass ratios for the "wet" aerosol particles, all particles should be expected to accumulate into smaller size bins upon evaporation of water. However, because of the deagglomeration effect, particles that have attained the constant mass ratio value have diameters, after evaporation, that lie in the smallest size bins. The particles whose mass is not changed significantly (such as in the AEROSIM-M code in the smaller size bins) have diameters, after evaporation, that are even smaller than that of the smallest size bin. Consequently, these particles are essentially lost from the particle size distribution.

The AEROSIM-M and the CONTAIN code results in Fig. 25 indicate that the MnO/CsOH mass ratio will increase with time for the airborne aerosol and for the cumulative settled aerosol. As seen from the preceding figures, the mass ratio of the larger airborne particles initially is relatively low, and the mass ratio of the settled particles is also low at early times. The average mass ratio of the airborne aerosol will increase as these larger particles settle faster than the smaller particles, and the mass ratio of the settled particles will also increase.

Aerosol Deagglomeration

In the preceding discussions, the seemingly anomalous behavior predicted by some results from the two CONTAIN codes was attributed to an apparent deagglomeration phenomenon. As a further example of such behavior, in the CONTAIN(ORNL) code output the airborne aerosol (MnO and CsOH) concentration in the smallest bin was a factor of 40 less at 3,600 s than at 28,000 s, (3,600 s just precedes supersaturation and 28,000 s just follows supersaturation). Normally, aerosol concentration in this smallest bin would be lower at 28,000 s due to losses by agglomeration and deposition. Finally, in Figs. 19 and 20 for the CONTAIN(ORNL) results, particle sizes (for the dry aerosol) that are smaller than the minimum bin size used in the CONTAIN(ORNL) calculation have been produced. After evaporation of water, these very small particles do not appear in the particle size distribution (see Fig. 21), since the code does not account for any particles smaller than the minimum size bin.

As an explanation of these anomalous results, it was theorized (in the draft of this report) that seed water nuclei, which are a particular feature of the CONTAIN code, could be causing aerosol deagglomeration. As discussed in the CONTAIN manual,[8] seed water nuclei are introduced into the system to ensure either that condensation will result under appropriate atmospheric conditions or that the predicted rate of condensation is at a suitable level. The manner by which the seed nuclei may cause deagglomeration is described in Appendix A.

After our draft report was issued, a study was initiated by the Sandia National Laboratories (SNL) in which calculations were performed with CONTAIN using input conditions similar to those of the CONTAIN(ORNL) code. The results of this study were discussed at the LACE Technical Advisory Committee (TAC) meeting on July 9–11, 1986.[9] The study found that the same results were obtained whether or not the seed nuclei option was included. The particular results cited were the airborne aerosol concentration vs time and the particle size distribution at 60,000 s. This study also found that the CONTAIN model for evaporation of water from the aerosol underestimated the rate of evaporation. After modification of the evaporation model, calculations gave a unimodal, rather than bimodal distribution at 60,000 s, as shown in Fig. 21. A "numerical diffusion" effect, which arises from the use of finite difference schemes to solve equations such as those utilized to describe aerosol behavior, was suggested to be responsible for the aerosol deagglomeration phenomenon.

A discussion of the "numerical diffusion" effect is presented in Appendix B, in excerpts from private correspondence with personnel at SNL.[10] These excerpts also include discussions about seed nuclei, a "bug fix" (regarding residual water on aerosols) planned for CONTAIN 1.05 which will modify the bimodal nature of the late-time particle size distribution, and the effect of the number of bin sizes in the CONTAIN calculations. The correspondence with SNL confirmed the error which we found in the NAUA-4 and the REMOVAL diffusiophoresis models.[6,11] As seen in Appendix B, workers at SNL demonstrated that increasing the number of size classes from 20 to 30 reduced the errors in certain quantities due

to "numerical diffusion" by more than two orders of magnitude. With 20 size classes or bins, a critical threshold for condensation growth is exceeded, which amplifies certain consequences of "numerical diffusion." Personnel at SNL pointed out that the inconsistencies in the CONTAIN results that were noted in our report involve only a very small part of the suspended mass present at the time they are noted. While this is true, the small particles to which the inconsistencies pertain represent a significant fraction of the suspended mass at the later times. This is seen at 60,000 s in Fig. 21 where, because of the lower settling rates of the smaller particles, their concentration has exceeded that of the larger particles. If a significant fraction of these small particles were created as a result of "numerical diffusion", then discrepancies between the predicted and experimentally measured aerosol concentrations could possibly be observed at late times.

Additional code calculations and detailed examination of the results are necessary to determine the relative importance of the aerosol deagglomeration phenomenon. Although the deagglomeration phenomenon did not appear to have a significant effect on the predicted aerosol behavior in the LA2 pretest calculations, it may be consequential in other accident sequences.

6. SUMMARY

Pretest aerosol transport code calculations were performed to model the aerosol behavior expected in LACE test LA2. The objective was to compare the results of the various codes to each other rather than to experimental data. To facilitate this comparison, various code input parameters and conditions to be used by all code analysts were specified, as summarized in Sect. 2. Calculations were performed by nine different codes to simulate the behavior of aerosol injected into the CSTF vessel with two preexisting leaks. Two codes included the option of condensation of steam on the aerosol, and one code included cases both with and without steam condensation on aerosol.

The following statements summarize the major results of the code comparison effort for the LA2 pretest calculations.

1. Significant differences were found between the AMMD values reported by some of the codes and the values we calculated using the particle size distribution results. The differences are attributed to the variation in methods used to calculate the AMMD. To allow for meaningful comparisons with experimental impactor data, the codes should determine the mass-median diameter (which is used to calculate AMMD) in a manner consistent with its definition (i.e., that diameter below which 50% of the mass of the particle size distribution lies).

2. Of the seven "dry" (i.e., no condensation of steam on aerosol) calculations, five codes predicted similar time histories for the airborne aerosol concentration. Low aerosol concentrations were calculated by the remaining two "dry" codes. The NAUA-5 results were affected by an error in the leak rate that was input to the code. The MAAP-2.9 code predicted high levels of aerosol deposition, which resulted in low aerosol concentrations. The CONTAIN(ORNL) and CONTAIN(UK) codes predicted different behaviors of the airborne aerosol concentration, which may be attributed to the effects of steam condensation on the aerosol.

3. Four of the codes for which the relevant information was supplied calculated differences in aerosol plating that appeared to be related to differences in diffusiophoresis and thermophoresis models. An error was found in the equation used by the NAUA-4 and the REMOVAL codes for plating by diffusiophoresis. Additional information from the code analysts is needed to determine the causes of any other differences in the predicted aerosol plating.

4. All codes except the CONTAIN codes predicted similar behaviors of the AMMD, the GSD, the aerodynamic mean settling diameter,

and the particle size distribution. The differences in airborne aerosol concentration behavior predicted by the NAUA-5 code apparently did not significantly influence the calculation of these parameters. Again, inclusion of the option of steam condensation on the aerosol affected the predicted behaviors of these parameters in the CONTAIN(ORNL) and the CONTAIN(UK) codes.

5. An aerosol deagglomeration phenomenon was observed in the results of the CONTAIN codes under conditions of steam condensation on aerosol. "Numerical diffusion" has been reported to be the cause of the deagglomeration phenomenon. Additional code calculations and detailed examination of the results are needed to determine whether aerosol deagglomeration has a significant effect upon the predicted aerosol behavior in other accident sequences.

6. More detailed information, such as the values of input parameters and copies of computer input and output, was supplied by the code analysts for the LA2 pretest calculations than for the LA1 pretest work. However, in order to contribute to a more meaningful code-comparison effort, all code analysts are encouraged to supply complete requested information for future calculations.

7. ACKNOWLEDGEMENTS

We would like to thank the code analysts who participated in this study for their efforts and cooperation.

8. REFERENCES

1. L. D. Muhlestein, Hanford Engineering Development Laboratory, "Transmittal of LA2 Final Test Plan (LACE-TP2)," letter to LACE program participants, November 12, 1985.

2. J. H. Wilson, Oak Ridge National Laboratory, "Instructions for Pretest Calculations for LACE Test LA2," letter to LACE program participants, December 4, 1985.

3. J. H. Wilson, Oak Ridge National Laboratory, Addendum to Instructions for Pretest Calculations for LACE Test LA2," letter to LACE program participants, December 17, 1985.

4. Hans Häggblom, Studsvik Energiteknik AB, Sweden, letter to A. L. Wright, Oak Ridge National Laboratory, concerning LACE Test LA1 pretest calculations with MAAP-2.9, January 20, 1986.

5. H. Bunz and W. Schock, Aerosols, Liu, Pui, and Fissan, eds., published by Elsevier Science Publishing Co., Inc., Amsterdan, 1984, pp. 845–848.

6. Private communication from J. H. Wilson, Oak Ridge National Laboratory, to R. Sher, EPRI, San Francisco, May, 1986.

7. H. I. Avci, "Diffusiophoretic and Thermophoretic Deposition of Aerosols on Surfaces in Light Water Reactor Containments Following Severely Degraded Core Accidents," Paper 11.3, Proceedings of the International Meeting on Light Water Reactor Severe Accident Evaluation, Vol. 2, Sessions 10–18, Cambridge, Mass., Aug. 28 to Sept. 1, 1983, Stone and Webster Engineering Corporation, Boston, 1983.

8. K. D. Bergeron, et al., User's Manual for CONTAIN 1.0, A Computer Code for Severe Nuclear Reactor Accident Containment Analysis, SAND 81-1495, NUREG/CR-2224, Draft, July 1984.

9. K. D. Bergeron, Sandia National Laboratories, Oral presentation, LACE Technical Advisory Committee Meeting, Richland, Washington, July 9-11, 1986.

10. Private communication, letter from K. K. Murata, Sandia National Laboratories, to J. H. Wilson, Oak Ridge National Laboratory, August 22, 1986.

11. J. H. Wilson, Oak Ridge National Laboratory, Oral Presentation, LACE Technical Advisory Committee Meeting, Richland, Washington, July 9-11, 1986.

APPENDIX A

AEROSOL DEAGGLOMERATION BY SEED WATER NUCLEI

In the approach used to solve the differential equations describing aerosol behavior for "discrete" codes (such as CONTAIN), the assumption is made that in each size bin all particles have the same composition. Consequently, when a particle "grows" or "shrinks" into a particular bin (i.e., by agglomeration, condensation, or evaporation), its composition is averaged in with the overall composition of all particles in the bin. If pure water aerosol particles are added as seed nuclei in the CONTAIN code, then the composition in all bins must change due to the addition of water. Since more particles (i.e., the seed nuclei) have been added to the bins, the overall effect is to spread the initial mass of the aerosol material in a bin over a greater number of particles. Thus, if the water that had been added to the bin were then to be evaporated, the calculated diameter of the dry aerosol particles would be less than the calculated diameter before the water was added. That is, the seed nuclei have resulted in the fragmentation or deagglomeration of the original aerosol material.

APPENDIX B

THE CONTAIN CODE - EFFECTS OF NUMERICAL DIFFUSION, SEED NUCLEI, AEROSOL RESIDUAL WATER, AND NUMBER OF BIN SIZE CLASSES[a]

"With regard to seed nuclei, the operation of the seed aerosol provision in CONTAIN is also explained below. It is shown that disabling the seed nuclei provision has no discernable effect on the ORNL calculation discussed in your report on the LA-2 pretest results. The inconsistencies in the ORNL calculation which you note in your report and attribute to seed nuclei should be attributed instead to numerical diffusion.

To explore the sensitivity to numerical diffusion (which all codes employing discretizations of continuous equations suffer from), the usual approach is to change the nodalization, which in this case is the number of size classes. We show below that by increasing the number of size classes from the 20 in the original ORNL calculation to 30, the errors in certain quantities due to numerical diffusion can be reduced by more than two orders of magnitude. However, we note the late time suspended mass of solids in the calculation with 30 size classes is considerably less affected than the two order of magnitude number suggests and is reduced by only a factor of 3. This factor of 3 in suspended mass is a reasonable estimate of the effects of numerical diffusion in the ORNL calculation, although we feel that the typical effect due to numerical diffusion is or can be reduced well below this value. The reason that the factor of 3 is felt to be excessive is that with the 20 size classes in the ORNL calculation, a critical threshold for condensation growth has been exceeded. With 30 size classes this threshold is not exceeded. As we

---

[a]Excerpts from private correspondence from K. K. Murata, Sandia National Laboratories, to J. H. Wilson, Oak Ridge National Laboratory, August 22, 1986.

show below, the threshold dramatically amplifies certain consequences of numerical diffusion.

The inconsistencies in the ORNL calculation noted in your report are discussed in detail below. We note they involve primarily the small particle wing of the size distribution function and the mass directly affected by the inconsistencies appears to be in one case a small part and in the other cases a negligible part of the suspended mass at the time. In the calculation with 30 size classes discussed above some of the inconsistencies you have noted can be changed by two orders of magnitude with only a nominal change in the suspended mass of solids. This calculation shows that the errors associated with the inconsistencies do not amplify appreciably after the suspended mass evolves with time.

The ORNL results are of considerable interest, although the details may not be particularly relevant to LA2. We wish to point out, first of all, that there will be a bug fix regarding residual water on aerosols in CONTAIN 1.05 which reduces significantly (but does not completely eliminate) the bi-modal nature of the late time size distribution found in the ORNL calculation. (It however has only a factor of two effect in reducing the late time suspended mass of solids.) Also, there are significant departures in the thermal hydraulic conditions in the ORNL data set from that specified by the test plan and that when these are corrected to the test plan the results change considerably. For example, the bi-modality disappears even without the bug fix. In addition, the calculated late time suspended mass increases by over an order of magnitude. We have unfortuantely not had time to look at the actual test conditions to see where they lie with respect to the test plan. You should however, expect a significant change between the pre- and post-test results.

(2) Seed Nuclei:

As you have noted in your draft report, there are inconsistencies in the particle size distributions in the ORNL LA2 pretest aerosol results. You attribute these to the CONTAIN seed aerosol provision. By disabling the seed aerosol provision, we have shown that the inconsistencies you attribute to seed aerosols are not due to the seed. Rather, they are

manifestations of numerical diffusion. This numerical diffusion is an unavoidable consequence of the finite difference methods currently used in CONTAIN, although we feel that in most cases the consequences of numerical diffusion on the suspended mass can be readily assessed and appear to be acceptable with a reasonable number of nodes. Other difference methods such as used for example in NAUA also have numerical diffusion but the characteristics of the numerical diffusion are somewhat different. An improved version of MAEROS is currently under development, which should suffer much less from numerical diffusion.

The lines of code in CONTAIN pertaining to the introduction of seed nuclei are A-CNTRL.100 through A-CNTRL.102. We note first of all that seed aerosol are introduced only if condensing conditions are present and the suspended mass in the first size class is zero. The material introduced is water, and the amount introduced is very small, typically .02 to .001 of the error tolerance used per timestep to integrate the mass concentration in each of the size classes. To put this another way, when the code finds a zero mass concentration in the first size class, the uncertainty in that zero due to integration error is 50 to 1,000 times larger than the amount of seed nuclei the code introduces.

The introduction of seed nuclei is a relatively infrequent occurence. Under condensing conditions for the smallest particle classes, the code tends to leave too much mass behind when calculating the number of particles which grow too large for their present size class and must be moved into the next size class. This result leads to numerical diffusion of the trailing edge of the distribution, which is a characteristic of the donor differencing used to calculate the promotion of particles to the next size class under condensing conditions. (We use donor rather than the more accurate but occasionally unstable central differencing under condensing conditions.) Therefore, the mass concentration of particles in the smallest size class generally does not zero out under conditions dominated by condensation, and once the condensation process starts, seed nuclei are not introduced very frequently. We in fact view seed nuclei primarily as a convenience to the user who encounters condensing conditions but has not specified any initial aerosols to condense on up to that point in the problem.

To demonstrate that the ORNL results are not sensitive to the seed nuclei provision, we have disabled it and instead specified an infinitesimal amount of water as an initial condition at the beginning of the preheat period. This initial condition is necessary because when the preheat steam is first turned on, condensation on aerosols occurs for a brief time. We do not believe that this initial amount of condensed water affects the dynamics of the aerosol of the aerosol solids introduced later. (The mass of the solids is much larger than the residual amount of condensed water left over from the preheat period.) When condensing conditions are encountered a second time, the solid aerosols have already been introduced and provide sites for the condensation to proceed. The attached Fig. 1 shows the particle size distribution found at 60,000 seconds using the ORNL data set and CONTAIN 1.04 without the seed provision. The total suspended mass is not discernably different from that given in your report and the distribution is almost identical to the distribution in your report. (The shift in the two curves is due to the fact that we have plotted the mass fraction in each size class, whereas you have applied a continuum normalizing factor to your curve.) We conclude that the results are not sensitive to seed aerosols.

(3) Numerical Diffusion:

Several inconsistencies are noted in your LA2 report with respect to the behavior of the amount and nature of the solid present in small particles composed of a mixture of water and solids. For example, on page 52 you note the fact that Figs. 19 and 20 show there are particles present with solid cores which are smaller than the smallest size solid particles in the sources in the problem. We believe that these inconsistencies are a manifestation of numerical diffusion. For example, the sub-minimum size of cores mentioned above is a manifestation of numericasl diffusion of the trailing edge of the particle size distribution as it moves to larger particle sizes under condensing conditions.

In order that this reduction in size of the solid cores not occur, the code would have to be able to treat a particle size distribution with a sharp cutoff on its trailing edge with absolutely no rounding of the cutoff. This appears almost impossible since the resolution of a size

class in CONTAIN is at best a factor of 2 in particle mass. The numerical problem is analogous to being able to propagate a discontinuous shock front through a discrete space mesh in a hydrodynamic calculation without smearing it and is recognized as a difficult one in the numerical analysis community.

From a practical point of view, which I take as being able to calculate suspended masses of solids to within a nominal factor of 2, the numerical diffusion may not make much difference. We have encountered calculations in the past which exhibit effects of numerical diffusion strongly in their size distribution functions but which are relatively unaffected with respect to suspended mass. Like these other calculations, the ORNL calculation exceeds a critical threshold with respect to condensation growth, as discussed below. Exceeding this threshold tremendously amplifies certain effects due to numerical diffusion. Nevertheless the presence of numerical diffusion in the ORNL calculation does not seem to affect the suspended mass by much more than the nominal factor of two.

We have increased the number of size classes in the ORNL data set from 20 to 30. This increase should reduce the numerical diffusion. (A slight increase in the upper particle diameter is necessary to introduce 30 classes and still satisfy the CONTAIN requirement of at least a factor of two variation in particle mass within a size class.) We have run this modified data set with CONTAIN 1.04. The resulting dry versus wet and the wet versus wet distributions at 10,000 seconds are shown in the attached Fig. 2. We recall that the condensation which started after the end of the source is still going on at this point.

We see from Fig. 2 that the solid mass in the small particle side of the dry versus wet distribution has been reduced by about an order of magnitude compared to the old results. Far more drastic that the change in the distribution of the solid is the change in the distribution of the condensed liquid. As you can infer from the wet versus wet distribution, the distribution of liquid in the small particle side of the distribution has been reduced by two and a half orders of magnitude. This is a tremendous reduction in the error due to numerical diffusion

The bi-modal distribution found at 60,000 seconds in the calculation with 20 size classes is preserved in the calculation with 30 size classes. Although this distributionn is not shown, the peak at large sizes is slightly more pronounced with the 30 size classes.

The calculated mass of the suspended solids as a function of time with 30 size classes is shown in the attached Fig. 3. The reduction in the amount of suspended solid at late time is a factor of 3 compared to the calculation with 20 size classes. Most of this reduction arises during the period between 8,000 and 14,000 seconds, during which condensation is occurring. The reason for the reduction is as follows: Condensation is preferentially occurring on the smaller particles present. The distribution reaches a quasi-steady state determined by agglomeration and settling of these smaller particles. As shown in Fig. 2, with 30 size classes, the agglomerating small particles carry more solid with them, and therefore the solid is more efficiently settled out.

The factor of 3 reduction in late time suspended solids is rather large compared to the variation we would expect in a dry problem with a change from 20 to 30 size classes. The change is large because we have crossed a critical threshold with respect to the number of size classes. As we have mentioned, the code tends to leave too much mass behind under condensing conditions. For an initial condition with mass present in only one size class, condensation should eventually move mass entirely out of that size class (i.e., the calculation should decrease the mass in that size class). However, if a critical threshold for condensation growth

$$m_{\ell+1}/m_{\ell} = 2.152$$

is exceeded, where m_{ℓ} is the particle mass at the ℓth size class boundary, the code will leave so much mass behind that growth of mass from the continuing condensation will occur in that size class as opposed to a decrease. This growth of mass is limited primarily by non-linear effects, such as Brownian agglomeration. For the 20 size class calculation,

$m_{\ell+1}/m_\ell = 2.818$, and for the 30 size class calculation, $m_{\ell+1}/m_\ell = 2.00955$. The 20 size class calculation is therefore unstable with respect to condensation growth, whereas the 30 size class calculation is not. The existence of this critical threshold was first noted by Dave Williams (Reference 4).

(4) Specific Comments on ORNL Draft Report:

We have looked at some of the inconsistencies specifically noted in your report by comparing the results using 20 size classes with those using 30 size classes. The first thing apparent about these inconsistencies is that they involve only a very small part of the suspended mass present at the time they are noted and this point should be stated in your report. For example, you note on page 52 that Figs. 19 and 20 show there are small composite particles present in the particle size distribution which have solid cores that are smaller than the minimum size (0.1 micron) of solid particles in the sources in the problem. We note that although such cores are present, the mass of such cores is negligible compared to the total suspended solid mass. (The dry versus dry distribution function for particles less than .1 micron is down by at least three orders of magnitude compared to the peak value.) As we have indicated above, this artificial reduction of core size is due to numerical diffusion. The amount of numerical diffusion can be changed by the nodalization. For example, the use of 30 size classes reduces the amount of solid mass in such cores by a factor of about 4.

In addition to this first inconsistency, which occurs under condensing conditions, there are two additional inconsistencies noted in your report which we would attribute to numerical diffusion of the leading edge (small particle side) of the size distribution under evaporating conditions. The second inconsistency is mentioned on p. 53 of your report and refers to Fig. 23 for the MnO/CsOH ratio on the ORNL calculation. In this Fig., the larger MnO/CsOH ratio found on the small particles relative to the large particle at 10,000 seconds is found to have leveled out at 60,000 seconds. The third inconsistency is mentioned on p. 55 of your report and is that in the ORNL calculation the amount of solids found in the smallest size class at 28,000 seconds exceeded the amount provided to that size class by sources in the problem.

In the ORNL calculation, evaporating conditions start just before 28,000 seconds. The evaporating conditions would tend to move the particle size distribution to smaller particle sizes. The leading edge (small particle side) of the distribution would be subject to numerical diffusion much like that which affects the trailing edge. Because we use central differencing on the leading edge under evaporating conditions, the numerical diffusion of the leading edge is much more controlled than with donor differencing. However, the central differencing does not eliminate numerical diffusion. The diffusion of the leading edge would tend to place solid mass from the large size classes into the small size classes.

This fact would, for example, explain the second inconsistency, the leveling of the MnO/CsoH ratio in ORNL calculation in Fig. 23 between 10,000 seconds and 60,000 seconds. At 10,000 seconds, the ratio as a function of size is similar to the AEROSIM calculation without condensation. For large particles there should be a leveling out of the ratio as shown because of agglomeration of small particles with large particles. Small particles, however, by virtue of their size could not have agglomerated with large particles bearing less than the average amount of MnO and a larger than average ratio should persist. In Fig. 23 the larger than average ratio persists for particles less than 1 micron in diameter at 10,000 seconds. However, at 60,000 seconds the ratio has almost completely leveled out.

In the calculation with 30 size classes, the complete leveling of this ratio still occurs. However, the importance of the complete leveling can be assessed looking at the dry versus wet distribution of Fig. 20. We see that the solid mass involved in particles of less than 1 micron is negligible--at 10,000 seconds, for particles in this size range, the dry versus wet distribution is down by at least six orders of magnitude compared to the peak value of the distribution. A small amount of diffusion of solids from particles of larger sizes could therefore very easily swamp the value of the ratio initially present for small particles. Since at 10,000 seconds the solid mass in the particles with larger than average ratios involved is negligible, the leveling out of the ratio for these particles appears to be irrelevant.

The third inconsistency is somewhat more disturbing. This inconsistency is that the solid mass in the smallest size class at one point in the calculation exceeded the amount provided by sources to that size class. In the ORNL calculation this happened at 28,000 s, at which time the mass in the first size class is a factor of 40 larger than that present near the end of the source at 3,000 s. At 28,000 s the fraction of the suspended solid mass represented by the smallest size class is about 5%. In the 30 size class calculation, the situation is improved considerably. At 28,000 seconds, the mass in the smallest size class exceeds the amount at 3,000 seconds by only a factor of 2, and the mass in the particle size range equivalent to the smallest size class in the 20 cell calculation is comparable to the corresponding quantity at 3,000 seconds. There appears to be a dramatic reduction of 40 in the amount of solid mass present at the smallest sizes at 28,000 seconds in going from 20 to 30 size classes.

We conclude that since the inconsistencies you have pointed out can be changed by orders of magnitude with only a nominal change in the suspended mass, their presence in the ORNL calculation is not a good indicator of a large error in the calculated suspended mass of solids. However, prudence dictates that a sensitivity study with respect to nodalization should be carried out, with nodalization adequate to prevent exceeding the critical threshold for condensation growth, whenever such inconsistencies are found.

Reference

4. D. C. Williams, Sandia National Laboratories, Internal Memo to K. Bergeron and K. Murata, Sandia National Laboratories, January 11, 1985.

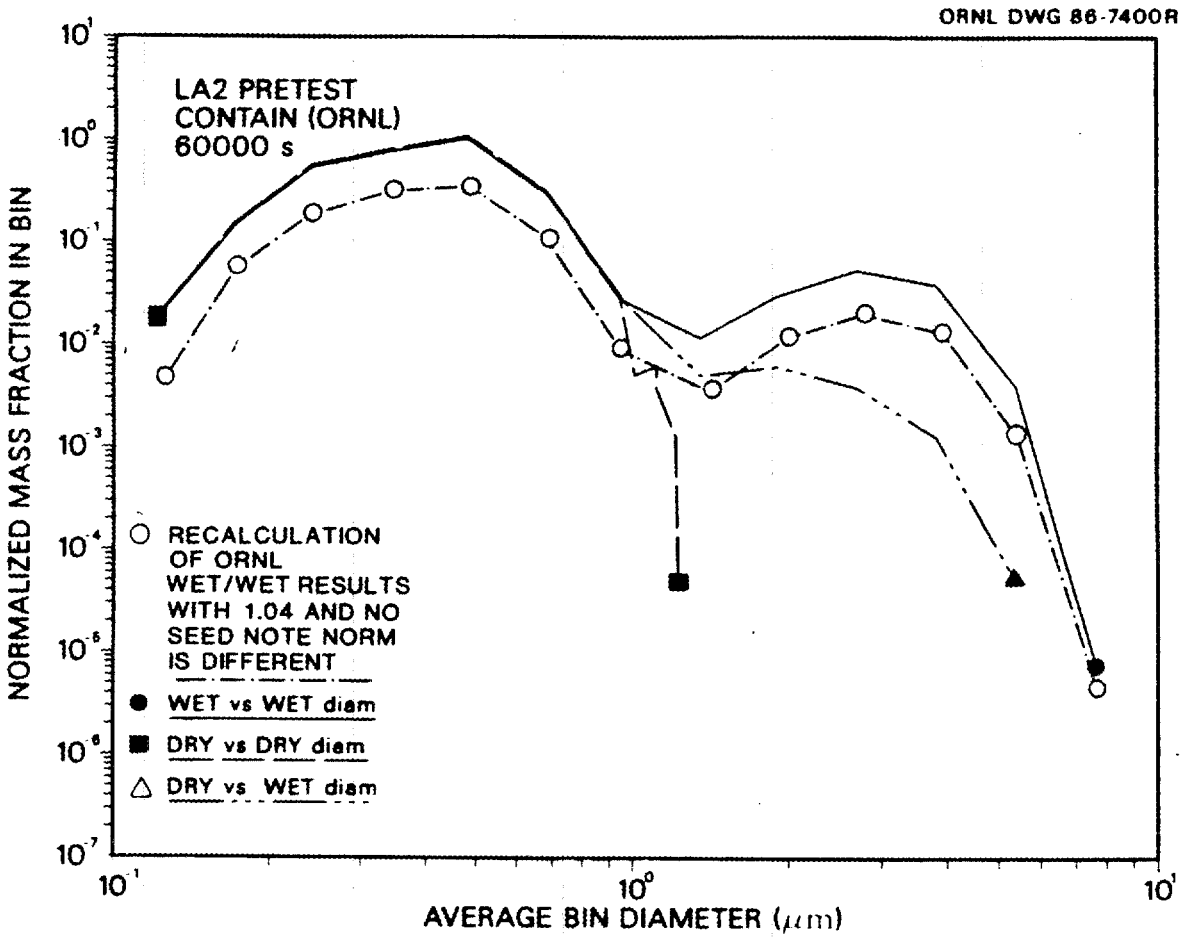

Fig. 1. Particle size distribution of airborne aerosol at 60000s for CONTAIN(ORNL) code.

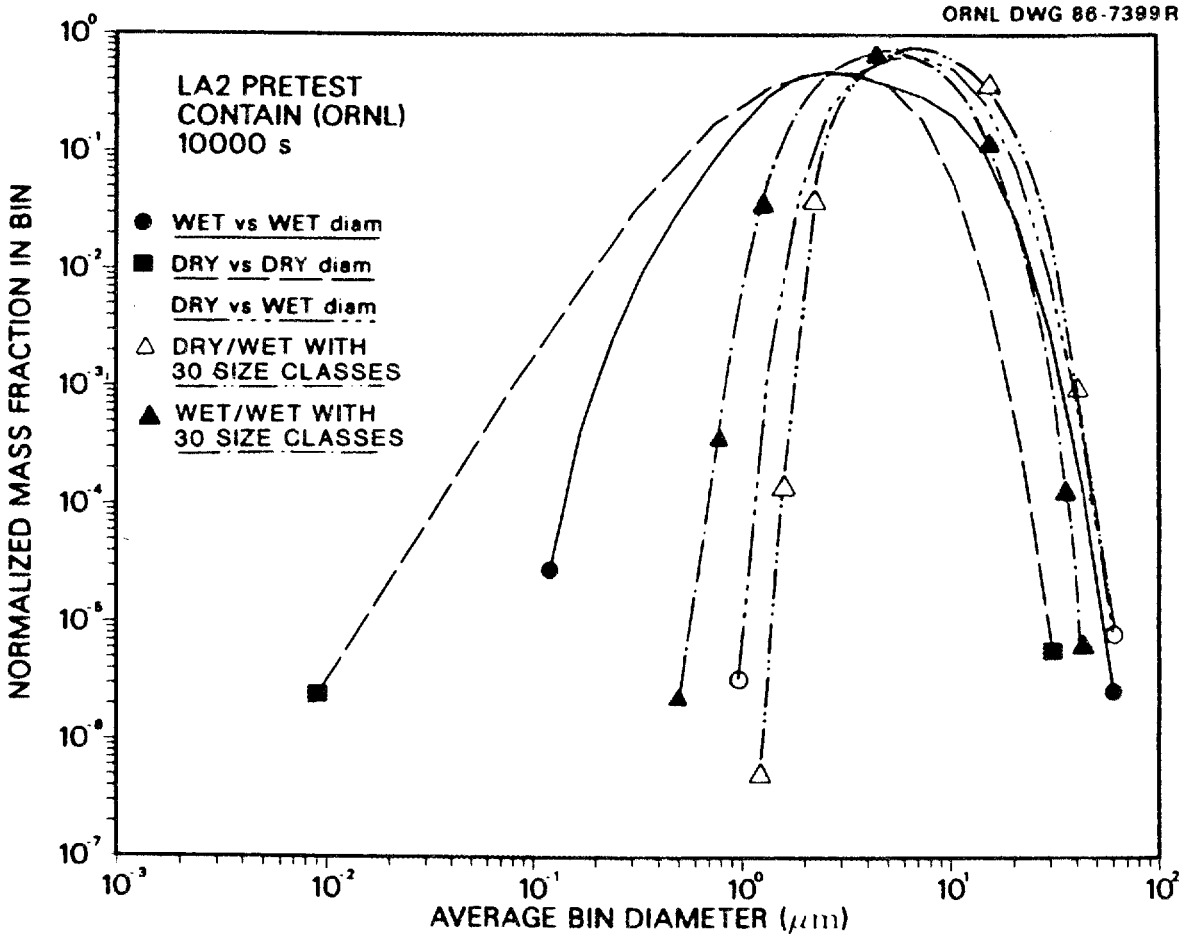

Fig. 2. Particle size distribution of airborne aerosol at 10000s for CONTAIN(ORNL) code.

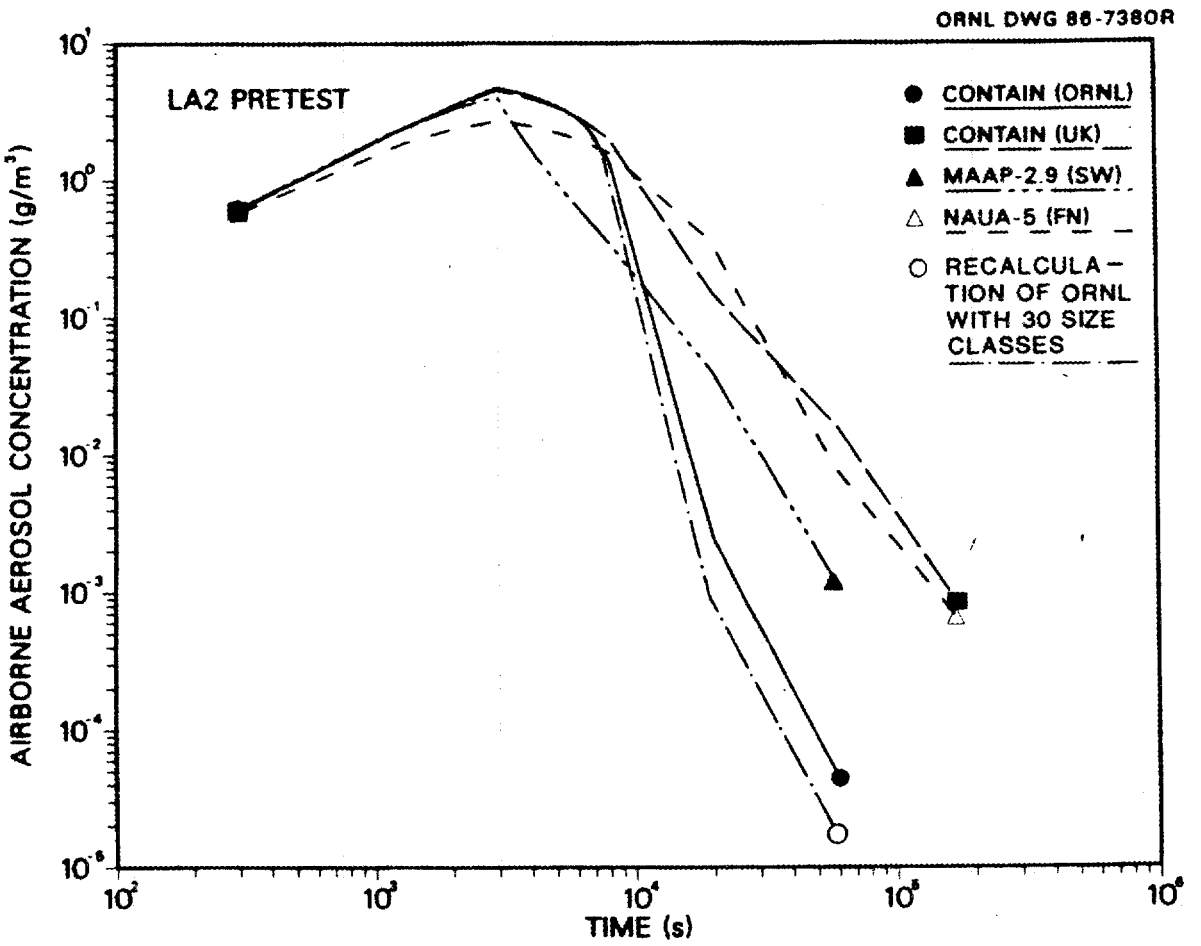

Fig. 3. Airborne aerosol concentration vs time - group 1.

INTERIM DISTRIBUTION

1-3. P. C. Arwood
4. L. H. Bell
5. J. R. Hightower, Jr.
6. E. K. Johnson
7. T. S. Kress
8. R. A. Lorenz
9. A. P. Malinauskas
10. F. R. Mynatt
11. M. G. Stewart
12-14. J. H. Wilson
15. A. L. Wright
16. R. G. Wymer
17-18. Technical Information Center
19. Office of Assistant Manager, Energy Research and Development, Oak Ridge Operations Office, Oak Ridge, Tennessee.
20. Laboratory Records - RC
21. ORNL Patent Section
22. Central Research Library
23. Document Reference Section